ARCHIVIO ISTITUZIONALE
DELLA RICERCA

Alma Mater Studiorum Università di Bologna
Archivio istituzionale della ricerca

Sedimentological analysis of ash-rich pyroclastic density currents, with special emphasis on sin-depositional erosion and clast incorporation: The Brown Tuff eruptions (Vulcano, Italy)

This is the final peer-reviewed author's accepted manuscript (postprint) of the following publication:

Published Version:
Lucchi, F., Sulpizio, R., Meschiari, S., Tranne, C.A., Albert, P.G., Mele, D., et al. (2022). Sedimentological analysis of ash-rich pyroclastic density currents, with special emphasis on sin-depositional erosion and clast incorporation: The Brown Tuff eruptions (Vulcano, Italy). SEDIMENTARY GEOLOGY, 427, 1-23 [10.1016/j.sedgeo.2021.106040].

Availability:
This version is available at: https://hdl.handle.net/11585/849294 since: 2022-11-22

Published:

DOI: http://doi.org/10.1016/j.sedgeo.2021.106040

Terms of use:

Some rights reserved. The terms and conditions for the reuse of this version of the manuscript are specified in the publishing policy. For all terms of use and more information see the publisher's website.

This item was downloaded from IRIS Università di Bologna (https://cris.unibo.it/).
When citing, please refer to the published version.

(Article begins on next page)

07 November 2026

This is the final peer-reviewed accepted manuscript of:

F. Lucchi, R. Sulpizio, S. Meschiari, C.A. Tranne, P.G. Albert, D. Mele, P. Dellino, Sedimentological analysis of ash-rich pyroclastic density currents, with special emphasis on sin-depositional erosion and clast incorporation: The Brown Tuff eruptions (Vulcano, Italy), Sedimentary Geology, Volume 427, 2022, 106040

The final published version is available online at ***https://dx.doi.org/10.1016/j.sedgeo.2021.106040***

Terms of use:

Some rights reserved. The terms and conditions for the reuse of this version of the manuscript are specified in the publishing policy. For all terms of use and more information see the publisher's website.

This item was downloaded from IRIS Università di Bologna (https://cris.unibo.it/)

When citing, please refer to the published version.

Revised manuscript with no changes marked

Click here to view linked References

Sedimentological analysis of ash-rich pyroclastic density currents, with special emphasis on sin-depositional erosion and clast incorporation: the Brown Tuff eruptions (Vulcano, Italy)

F. Lucchi [a, *], R. Sulpizio [b, c, d], S. Meschiari [a], C.A. Tranne [a], P.G. Albert [e,f], D. Mele [b], P. Dellino[b]

[a] Dipartimento di Scienze Biologiche, Geologiche e Ambientali, Università di Bologna, Piazza Porta S. Donato 1, 40126 Bologna, Italy

[b] Dipartmento di Scienze della Terra e Geoambientali, Universitá di Bari, via Orabona 4, 70125 Bari, Italy

[c] INGV- Bologna section, via D. Creti, 40100, Bologna, Italy

[d] IGAG-CNR, Area della Ricerca di Roma 1- Strada Provinciale 35d, Montelibretti (Rome), Italy

[e] Department of Geography, Swansea University, Singleton Park, Swansea SA2 8PP, UK

[f] Research Laboratory for Archaeology and the History of Art (RLAHA), University of Oxford, Dyson Perrins Building, South Parks Road, Oxford OX1 3QY, UK

[*] Corresponding author

ABSTRACT

The sedimentological, lithological and textural characteristics of the Brown Tuffs (BT) pyroclastic deposits, combined with their grain-size, componentry and geochemical glass compositions, are here investigated to obtain information on the transport and depositional mechanisms of the corresponding pyroclastic density currents (PDCs). The BT are widespread reddish-brown to grey, ash-rich pyroclastic deposits generated by pulsating hydromagmatic explosive activity from the La Fossa Caldera on Vulcano island during the c. 80-6 ka time-stratigraphic interval, and then distributed on most of the Aeolian Islands and Capo Milazzo peninsula (Sicily) and in the Tyrrhenian and Adriatic Sea regions. Near the source area on Vulcano, the BT are characterised by alternating massive and

planar to cross stratified lithofacies that result from the stepwise, repeating aggradation of discrete PDC pulses. This alternance is regulated by either fluid escape or granular flow depositional regimes at high clast concentration or grain by grain traction deposition in the waning diluted stages of the PDCs. Most of the BT on Vulcano show intermittently stratified and massive ash deposits resulting from a pervasive post-depositional disruption of the primary structures. This is induced by upward fluid expulsion associated with dissipation of pore pressure between layers at different grain size (fine to coarse ash) and porosity, as outlined by distinctive upwards bends and pillar-type escape structures through the fluid-filled cracks and rupture points. Massive BT deposits with a faint colour and grain-size banding are widely recognised on Lipari, the nearby island of Vulcano. Based on the presence, at the base of BT depositional units, of cm-thick amalgamation bands containing pumice lapilli, scoria and lithic clasts ripped-up and embedded from the loose underlying pyroclastic units, they are interpreted as deposited by ash-rich PDCs laterally spreading from La Fossa Caldera and moving to Lipari. During their motion to Lipari these currents (likely) crossed a narrow and shallow sea-water inlet which did not stop their advancement but influenced the grain size distribution of those spreading on the Lipari mainland. In this paper, the mechanism of clast erosion and incorporation is outlined across the whole island of Lipari by means of field study, grain-size, and geochemical glass analyses on the different components of the mixed basal bands of the BT. This suggests that the BT PDCs maintained enough flow power as to erode the substratum, hence likely impacting the territory, over a distance up to at least 16-17 km from the volcanic source. Evidence that the BT PDCs exerted a high shear-stress over the loose substratum is also provided by undulated, recumbent flame and rip-up structures at the base of some depositional units in southern and central Lipari. In order to form such bed granular instabilities between the BT and the underlying deposits we calculate that the currents had at least a shear velocity of ca. 2 m s^{-1} and a shear stress in the range of 1-4.5 kPa. These results add new insights on the large-scale hazard at the Aeolian Islands and shed new lights on the widespread transport and depositional dynamics of ash flows spreading over the sea and reaching nearby islands, and their interactions with the substratum and the pre-depositional topography.

KEYWORDS

Brown Tuffs, Aeolian Islands, Sedimentary structures, Pyroclastic density current, Clast embedding, Shear-related granular instability structures

1. INTRODUCTION

Pyroclastic density currents (PDCs) are ground hugging mixtures of particles and gas that flow laterally across the topography, and are among the most amazing, complex and dangerous volcanic phenomena (e.g., Carey, 1991; Druitt, 1998; Branney and Kokelaar, 2002; Sulpizio et al., 2014; Lube et al., 2020). Irrespective whether they are concentrated or diluted, PDCs are characterised by a very hostile nature and a complex interplay between transport and depositional mechanisms, which make their study a great challenge for volcanologists. The only way we have to get information about the processes occurring at the time of deposition is to analyse the deposit lithofacies and lithofacies associations in the field (e.g., Sohn and Chough, 1989; Branney and Kokelaar, 2002; Sulpizio et al., 2008a, 2010) or to replicate PDCs in the laboratory (Dellino et al., 2007; 2010; Andrews and Manga, 2012; Sulpizio et al., 2016; Breard and Lube, 2017; Brosch and Lube, 2020). This is particularly demanding for ash rich PDCs that usually have a massive structure and homogeneous lithology, which make a unique sedimentological interpretation challenging. Furthermore, quite rare is in the volcanological literature the analysis of the interaction between PDCs and the pre-depositional topography, which can influence the runout and the internal organisation of the parent currents by means of the bulking due to substratum erosion (Roche et al., 2013; Bernard et al., 2014; Roche, 2015; Pollock et al., 2019).

The Brown Tuffs (BT) deposits, largely outcropping over the Aeolian islands and northern Sicily (Italy), represent an exceptional case-study for shedding light on the elusive processes that drive erosion and deposition in ash-rich PDCs, and their interactions with the substratum. The BT

79 are ash-rich, reddish-brown to grey volcaniclastic deposits from PDCs and associated fallout
80 produced over a long-time span by pulsating hydromagmatic eruptions from the La Fossa Caldera
81 on Vulcano island (Lucchi et al., 2008, 2013b; Cicchino et al., 2011; Meschiari et al., 2020). They
82 usually crop out as massive, moderately to well sorted, fine to coarse ash deposits of meter-scale
83 thickness. Their quite ubiquitous massive appearance, recurring over a wide time span in the
84 stratigraphy of the Aeolian Islands, and the paucity of distinctive sedimentological characteristics
85 have long made it difficult to define the eruptive and depositional mechanisms of the BT. As such,
86 they have been generically interpreted either as primary deposits from PDCs or fallout, reworked
87 deposits from wind-blown volcanic ash (tuff-loess) or even paleo soils (Bergeat, 1899; Keller, 1967,
88 1980a, 1980b; Pichler, 1980; Crisci et al., 1981, 1983, 1991; Manetti et al., 1988, 1995; Morche,
89 1988; Losito, 1989; Gioncada et al., 2003). According to the most accepted interpretation, they
90 were emplaced on Vulcano and southern Lipari islands by mostly dilute PDCs, based on the
91 occurrence of rare stratified lithofacies, internal colour and grain-size banding (fine to coarse ash)
92 and topography-controlled thickness variations (De Astis et al, 1997; Lucchi et al., 2008, 2013b;
93 Dellino et al., 2011; De Rosa et al., 2016), although more detailed information on the transport and
94 depositional behaviour of these PDCs has been missing so far. BT deposits cropping out in more
95 distal outcrops on the other islands of the Aeolian archipelago and the Capo Milazzo peninsula were
96 instead related to fallout from a pulsating eruption columns or co-ignimbrite ash clouds (Lucchi et
97 al., 2008).
98 We present here an in-depth field study of the lithological and sedimentological
99 characteristics of the BT in the proximal and medial-distal outcrops on Vulcano and Lipari islands
100 (Fig. 1A), with the aim of investigating in detail the transport and depositional mechanisms of the
101 corresponding PDCs. Special attention was paid to the evidence of erosion and clast incorporation
102 in the basal portions of some BT depositional units, which were previously signalled by Lucchi et
103 al. (2008; 2013b). Together with the occurrence of shear-related sin-depositional sedimentary
104 structures, this can provide information about the processes occurring in the basal portion of PDCs,

which transport the vast majority of the total flow mass (Branney and Kokelaar, 2002; Sulpizio et al., 2014) and determine the threat of these dangerous phenomena (Sulpizio et al., 2014; Dufek et al., 2015; Pollock et al., 2019). In recent times, the erosive capacity of PDCs and their ability to produce sin-depositional substrate deformation by shear forces was studied by means of observations in the field (e.g. LaBerge et al., 2006; Cas et al., 2011; Pollock et al., 2019; Doulliet et al., 2019) or small scale laboratory experiments (e.g. Roche et al., 2013), mostly focused on polydisperse, poorly sorted, concentrated PDC deposits (e.g. those related to the 1980 Mt. St. Helens eruption; Pollock et al., 2019). Nothing has been done, however, on the erosive capability of well sorted, ash rich PDCs. In order to contribute to bridging this gap, we carried out a detail field investigation of the lower portions of the ash-rich BT depositional units supported by grain-size, componentry and geochemical analyses, which helped in deciphering the depositional dynamics of BT PDCs and shed new light on the dispersal dynamics of ash-rich PDCs.

2. GEOLOGICAL SETTING

2.1. Aeolian Islands

The Aeolian Islands (Alicudi, Filicudi, Salina, Lipari, Vulcano, Panarea and Stromboli; Fig. 1B) are the emerged portions of an active volcanic system in the Southern Tyrrhenian Sea, which also includes several seamounts (Barberi et al., 1973; Beccaluva et al., 1985; De Astis et al., 2003; Chiarabba et al., 2008; Ventura, 2013). Aeolian volcanism entirely occurred during the Quaternary, as demonstrated by the oldest radiometric age of c. 1.3 Ma of submarine lavas from the Sisifo seamount (Beccaluva et al., 1985), and then developed subaerially from ~270-250 ka to historical and present times (Leocat, 2011; Lucchi et al., 2013b, and references therein) (Fig. 1C). Successive eruptive epochs of the different volcanic islands have been subdivided by volcanic collapses or major quiescent (erosional) stages (De Astis et al., 2013; Forni et al., 2013; Francalanci et al., 2013; Lucchi et al., 2013a, 2013c, 2013d, 2013e), sometimes associated with episodes of marine ingression and

terrace formation during the major sea-level fluctuations (Lucchi, 2009). The marine terraces attributed to the marine (oxygen) isotope stage (MIS) 5, dated between c. 124 and 80 ka (Chappell and Shackleton, 1986; Waelbroeck et al., 2002; Rohling et al., 2014), are well constrained time-stratigraphic markers on most of the archipelago. The erupted magmas in the Aeolian Islands range from basaltic andesites to rhyolites over a large range of differing magmatic suites from calc-alkaline (CA), high-K calc-alkaline (HKCA), shoshonitic (SHO) and K-Series (KS) (Ellam et al., 1988; Francalanci et al., 1993; Peccerillo et al., 2013). Major Violent Strombolian to Sub-Plinian eruptions involving dacite to rhyolite magmas have occurred on Lipari, Vulcano, Salina and Stromboli during the last glacial period (from c. 80 ka) and the early Middle Ages (Crisci et al., 1981; Hornig-Kjarsgaard et al., 1993; Keller and Morche, 1993; Colella and Hiscott, 1997; De Astis et al., 1997a, 2006). This is the time-stratigraphic period when the BT, the object of the present study, were erupted.

2.2. The Brown Tuffs

The BT are widespread, reddish-brown to grey, massive ash-rich volcaniclastic deposits with metric thickness recognised in the Aeolian Islands and the Capo Milazzo peninsula (Sicily).

Chemo-stratigraphic and tephrochronological studies by Lucchi et al. (2008, 2013b) and Meschiari et al. (2020) have documented the BT occurrence, with variable volumes and dispersal areas, on the islands of Vulcano, Lipari, Salina, Filicudi, Stromboli and Alicudi and the Capo Milazzo peninsula, and in Tyrrhenian and Adriatic Sea marine cores, in the c. 80-6 ka time-stratigraphic interval. The BT have been interpreted as the result of PDCs and associated distal fallout related to a pulsating hydromagmatic explosive activity from a source located inside the La Fossa caldera on Vulcano island (De Astis et al, 1997; Lucchi et al., 2008, 2013b; Cicchino et al., 2011) (Fig. 1A). Also, the composition of BT, ranging from K-series (K_2O = 3.3-7.5 wt.%) basaltic trachy-andesites and trachy-andesites through to tephri-phonolites and trachytes (SiO_2 = 49.9-64.1 wt.%; $Na_2O + K_2O$ = 6.5-12.6 wt.%), is entirely consistent with the Vulcano magmatic system (Meschiari et al., 2020).

The BT succession is delimited at the base by marine terraces attributed to the late marine (oxygen) isotope stage (MIS) 5 (c. 124-80 ka) and is subdivided into four macro-units: Lower BT (LBT; 80-56 ka), Intermediate BT (IBT; 56-27 ka), Intermediate-upper BT (IBT-upper; 26-24 ka) and Upper BT (UBT; 24-6 ka). This subdivision is based on the occurrence of interbedded widespread regional or local marker beds, namely the 'Ischia Tephra', equivalent to the Y-7 marine marker tephra (Epomeo Green Tuff, 56 ka; Keller et al., 1978; Tomlinson et al., 2014), the Monte Guardia pyroclastics from Lipari (27-26 ka) and the Spiaggia Lunga scoriae (24 ka) on Vulcano (Fig. 2) (Meschiari et al., 2020). These macro-units are furtherly split into (at least) 16 depositional units, best documented on Vulcano and Lipari islands, where they have variable thicknesses ranging from a few decimetres up to a maximum of 3 m (for each depositional unit), while the entire BT succession has a (cumulated) maximum thickness of 15–25 m on Vulcano and southern Lipari. The different BT depositional units are best distinguished when they are separated by interlayered (local) volcanic units and tephra layers. Between these, the Petrazza Tuffs from Stromboli (77-75 ka) contribute to define the lower chronological constraint of the LBT, whilst the Grey Porri Tuffs (GPT, 70-67 ka) and Lower Pollara Tuffs (LPT, 27 ka) from Salina and the Vallone del Gabellotto tephra from Lipari (8.7–8.4 ka) are important for stratigraphic subdivisions in the LBT, IBT and UBT, respectively (Fig. 2). The Cugni di Molinello scoria bed is an important stratigraphic marker on Vulcano separating the lower and upper portions of the UBT (De Astis et al., 1997; Lucchi et al., 2008, 2013b), which are delimited at the top by the Punte Nere tuffs (5.5 ka). A list of the main features of the units interlayered within the BT succession is provided in the Supplementary File 1. When not intercalated with other deposits, the BT generally appear as lithological homogeneous tephra accumulations that are unlikely to represent single depositional units, but instead they are the amalgamation of different depositional units, as also testified by the occurrence of interlayered localized erosional surfaces and reworked horizons with a limited lateral persistence.

3. METHODS AND TERMINOLOGY

Lithostratigraphic and sedimentological analysis of the BT was carried out on most of the outcrops exposed on the islands of Vulcano and Lipari (Fig. 1A; Table 1), which allow identification (and correlation) of the largest number of depositional units of the BT, relative to all the distinguished BT macro-units (LBT, IBT, IBT-upper and UBT). Following Lucchi (2013), a "depositional unit" is defined as the volcanic (pyroclastic) material deposited during a single, relatively continuous depositional event from PDCs or fallout, and is delimited by evidence of interruptions of deposition (e.g. erosive surfaces, paleo soils, reworked beds, angular discordances) or other sedimentological features (e.g. presence of fine "co-ignimbrite" ash, lithic-rich beds, sharp grain-size variations), and/or by interlayered exotic pyroclastic (including distal tephra layers) or lava deposits.

Outcrop description and sediment logging were based on classical lithostratigraphy and lithofacies analysis, as the main tools to infer the volcanological interpretation of the studied deposits in terms of their transport and emplacement mechanisms (see Branney and Kokelaar, 2002; Sulpizio and Dellino, 2008; Lucchi, 2013 for reviews). Sedimentological investigation of BT units was carried out through lithofacies analysis, which has commonly been used to describe and decipher the deposits of marine and non-marine environments (e.g. Miall, 1978; Lowe, 1982; Mathisen and Vondra, 1983; Miall, 1985; Smith, 1986, 1987; Waresback and Turbeville, 1990; Zanchetta et al., 2004a) and then applied to complex sequences of pyroclastic deposits (Sohn and Chough, 1989; Chough and Sohn, 1990; Colella and Hiscott, 1997; Gurioli et al., 2002; Sulpizio et al., 2007, 2010) and to lateral and vertical variations of sedimentary structures within widespread ignimbrites (e.g. Freundt and Schmincke, 1986; Druitt, 1992; Cole et al., 1993; Allen and Cas, 1998). Lithofacies have been identified in the BT deposits using a combination of texture, sedimentary structures, grain-size and sorting (Table 2). Sedimentary structures were described and measured at cm-scale, and grain-size and component analyses were carried out on selected samples of the mixing bands and reworked bed material at the base of various BT depositional units. Weight % of the size fractions coarser than 3 ϕ (125 μm) at 0.5 ϕ intervals ($\phi = -\log_2 d$), where d is the particle size in mm) were estimated using dry

208 mechanical sieving. The finer fractions, from 3.5 ϕ (63 μm) to 9 ϕ (2 μm), were analysed by means
209 of a Beckman Coulter Multisizer 4 (Mele et al., 2015), and expressed as volume % and successively
210 converted in weight % using a constant clast density assumed equal to that of powdered BT.
211 Component analysis (juvenile, lithics and crystals) was carried out on a representative number of
212 particles of each grain-size fraction of the bulk material. We have differentiated six main classes of
213 components in the size fractions coarser than 3 ϕ (125 μm): i) pumice (white and grey) and ii) scoria
214 of different porphyricity and vesicularity; iii) obsidian fragments; iv) glass fragments; v) crystals; vi)
215 lithic clasts. The finer size fractions are undifferentiated. For the size fractions in the range from 16
216 to 1.4 mm, a subsample of particles of each component was hand-picked and weighted; the weight
217 fraction of each component was calculated for each size by scaling the number of particles of the
218 subsample to the total weight of the sample. For the grain-size range from 1 to 0.125 mm, particles
219 of each component were counted under a stereomicroscope. The weight of each component was
220 estimated by means of the density of each component in each size fraction. The grain-size statistical
221 parameters by Folk and Ward (1957) were then calculated for the different sub-populations
222 recognised in the samples from the base of BT depositional units by means of the GRADISTAT
223 program (Blott and Pye, 2001; Table 3).

224 Major and minor element glass data for selected samples of the basal portions of a number of
225 BT depositional units are here provided, referring to the extensive dataset recently made available by
226 Meschiari et al. (2020) for most of the BT depositional units and the interbedded tephra deposits. The
227 samples were mounted in Streurs Epofix epoxy resin and mounts were ground, polished and carbon
228 coated in preparation for chemical analysis. Glass data were determined using a wavelength-
229 dispersive JEOL 8600 electron microprobe (WDS-EMP) hosted at the RLAHA, University of
230 Oxford. Details of the analytical operating conditions, monitoring of data accuracy and precision, and
231 post-analysis data treatment are provided in Meschiari et al. (2020), together with the MPI-DING
232 reference glasses (Jochum et al., 2006). Data presented in plots are normalised (e.g., water-free) and

error bars represent reproducibility, calculated as 2X standard deviation of replicate analysis of StHs6/80-G reference glass.

4. RESULTS AND ANALYSES

4.1. Sedimentological features of the BT

Sedimentological analysis of the BT has been carried out on the outcrops exposed on Vulcano and Lipari islands (Fig. 1A), which allow definition of the most complete succession of distinct depositional units of the LBT, IBT, IBT-upper and UBT macro-units (Fig. 2). Most of the outcrops are located in the flattish area of Il Piano on Vulcano island, located southeast of the La Fossa Caldera source area, and mainly belong to the UBT macro-unit. These outcrops are the most proximal today exposed, because the very proximal BT deposits within the inner part of the La Fossa Caldera were affected by the recent collapses in this area or buried below the Holocene deposits of the La Fossa cone (De Astis et al., 2013). Other outcrops of the BT are located to the west of the La Fossa Caldera, near the locality of Grotta dei Pisani, and along the southern flank of Vulcano, near Gelso (Fig. 1A). The BT have been also investigated on a number of outcrops in distinct sectors of the nearby island of Lipari at increasing distances from the source area. The main characteristics of the studied outcrops, and their distance from the source area, are summarized in Table 1.

In most outcrops the BT consist of massive (fine to coarse) ash and show, in places, internal bands of different colours (and grain-size) with gradual contacts (lithofacies mA; Table 2; Fig. 3A). Plane-parallel to cross bedding stratification and lamination (lithofacies psA-xsA; Table 2; Fig. 3B) occur in some exposures on Vulcano and southern Lipari islands, particularly in the UBT deposits (De Astis et al, 1997; Lucchi et al., 2008). Dune bedding with internal cross stratification (having ca. 2-m wavelength and 0.5-m amplitude) are observed in the outcrops of the UBT outside the south-eastern rim of La Fossa Caldera. In the outcrops on Vulcano island, the BT are generally characterised

by the alternation of mm to cm thick massive and stratified beds (lithofacies altpsmA), with the occurrence of some laminae of weakly consolidated reddish fine ash. The stratification (and lamination) is generally not laterally persistent and is largely disrupted (lithofacies isA; Table 2; Figs. 3C-F). A typical upward bending of the laminae is observed in many of the fragmentation points (Fig. 3E-H), and in some cases disruption of the laminae occurs in correspondence of mm-scale vertical columns of coarse ash (Fig. 3G-H). The disruption of stratification (lamination) is frequently pervasive, with fragments of laminae distributed unevenly within the massive deposits. It is noteworthy that in a number of outcrops on Vulcano, although seemingly not stratified and unstructured, the BT deposits embed scattered fragments of laminae as relicts of the original stratified/laminated lithofacies (Fig. 3I).

Sin-depositional shear structures (lithofacies mixAL, ucAL, rfAL, ruAL; Table 2) are described and measured at cm-scale at the base of most of the BT depositional units (Figs. 4 and 5), and they are mainly recognised on Lipari rather than on Vulcano (the BT source area). This is probably because of the most common occurrence of interlayered (incoherent) exotic pyroclastic deposits within the BT succession on Lipari, which make the shear structures in the basal portions of the different BT depositional units more evident. In these cases, the basal contacts between BT and exotic deposits are transitional (Fig. 4) and occur as bands of mixed material between the BT and the underlying incoherent pyroclastic deposit (lithofacies mixAL; Table 2). Most of the interbedded pyroclastic deposits are composed of whitish to grey pumice and obsidian of local origin (Punta di Perciato, Falcone, Lip1, Monte Guardia, Vallone del Gabellotto) or grey to dark-grey scoriae and pumice from Salina (Grey Porri Tuffs and Lower Pollara Tuffs), which show a strong lithological contrast with respect to the homogeneous reddish-brown to grey, ash characterizing the BT (Fig. 4). Where two BT depositional units directly overlie each other without a distinguishing layer of exotic pyroclasts, the original thickness and limit between the units cannot be easily recognised (e.g., Fig. 3A), unless it is marked by a minor erosive surface, as occurs in places (Lucchi et al., 2008). This seems the case of the island of Vulcano where the succession of BT is generally made up of distinct, amalgamated

depositional units, interlayered only occasionally with exotic pyroclastic deposits. On Vulcano, visible mixing bands occur only when BT units overlie the whitish pumice lapilli and ash of the Monte Guardia and Vallone del Gabellotto fall deposits (Fig. 4G, H) or dark-grey scoriae of the Cugni di Molinello unit. Note that the base of the BT depositional units is sharp when they overly lavas or welded scoriae and other non-erodible pyroclastic deposits, whilst the top contact of BT where they are overlain by other exotic deposits is always sharp (conformable or unconformable).

Over the entire study area (from northern Lipari to southern Vulcano) the lithofacies mixAL occurs independently of the paleo-topography, outcropping even in case of a sub-horizontal paleo topography. Thickness of the mixing bands ranges (approximately) from a few to tens of cm, with a gradual upward transition to the un-mixed BT material (Fig. 4; Table 1) and is arbitrarily measured relative to the level where the original component of BT is dominant with respect to the incorporated clasts from the underlying units. The mixing bands are generally massive, but they show in places alignments of lapilli. The maximum dimension of entrained clasts (either pumice, scoria or lithic) is generally of fine to medium lapilli, although they can occasionally reach sizes of 10 cm (e.g., at the base of BT9 depositional unit in southern Lipari; Fig. 4E). The entrained clasts may be uniformly distributed within a whole BT depositional unit, even if scattered (e.g., Fig. 4F), but in most cases their abundance decreases regularly upwards. When the range of grain sizes of the entrained clasts is broad, reverse grading of the coarse clasts is observed (e.g., Fig. 4E).

Undulated structures consist in basal layers composed of mixed material between the BT and the underlying incoherent pyroclastic deposit that appear as wavy and consisting of alternating crests and troughs (lithofacies ucAL; Table 1). They are recognised in southern and central Lipari at the contact between BT and the underlying pumice units (Fig. 5A-C). Following Pollock et al. (2019), the length of an undulated structure is the distance between successive troughs, and its height is the distance from the lowest part of a trough to the top of the crest. Undulated structures on Lipari have length between 60 and 450 cm and height of ca. 20 cm (Table 1), and they are best exposed in outcrops arranged longitudinally with respect to the BT source area, at distances of 7-10 km (Fig. 5A-C). Crests

311 are almost symmetric and internally massive (Fig. 6B), showing imbrication of coarser clasts in the
312 upper part of the mixed material.

313 Recumbent flame structures (lithofacies rfAL; Table 2) have an overhanging arm of entrapped
314 clasts from the basal layer that protrudes up into the BT deposit and becomes sub-horizontal and thins
315 in downflow direction (conforming with Pollock et al., 2019). They look very similar to the 'shark
316 fin' structures of Douillet et al. (2019). Recumbent flame structures are common at the base of
317 depositional unit BT9, with the best preserved one documented above the Falcone pyroclastic
318 deposits at Spiaggia Valle Muria, south of Lipari, where the structure has a length of about 60 cm and
319 height of about 20 cm (Fig. 5D). The length is the extent of the deformed zone and the height is the
320 distance from root to top of the sub-horizontal tail. Lithofacies rfAL commonly occurs as trains of
321 pumice and lithic lapilli a few cm above and parallel to the basal contact of the depositional unit BT9
322 (Fig. 5D). In places, only the trunk of the structure is preserved as an asymmetric deformation of the
323 lapilli from the underlying bed (Fig. 5E).

324 Rip-up structures (lithofacies ruAL; Table 2), similar to recumbent flame structures, are visible
325 at the base of some depositional units. In these cases, the contact is almost planar, but there are small
326 hook-like structures as asymmetric deformations of the underlying bed, which resemble the trunk of
327 a flame structure (Fig. 5F). These structures are usually few cm in height, and they are bended
328 downcurrent.

329

330

331 **4.2. Grain-size and components of the mixing bands of the BT**

332 We collected samples of the mixing bands at the base of some BT depositional units on Lipari
333 island, with the aim of investigating their grain-size distribution and components. The depositional
334 units investigated here cover mostly the stratigraphic interval of the IBT and IBT-upper macro-
335 units, but, as for the grain-size distributions, the results may be considered representative of the

entire BT succession because of similar lithology and textural characteristics (Lucchi et al., 2008; De Rosa et al., 2016).

Most samples have a polymodal grain-size distribution (except for sample Lip03/17) and a large number of components (Fig. 6), as widely expected for mixing bands between BT units and the underlying tephra beds. In this respect, each grain-size distribution is the combination of two distinct sup-populations of components, one referred to the BT and the other relative to the underlying pyroclastic deposits. Considering that the Folk and Ward (1957) statistical parameters, like median diameter (Mdϕ) and sorting (σϕ), are not useful for polymodal distributions, we then calculate them in Table 3 for the separated component distributions (and not for the bulk grain-size) recognised in the samples from the base of BT depositional units as in Figure 6.

The BT typically consist of fine (dominant) to coarse ash composed of aphyric, glass fragments (from about 65 to 90 vol. %), from dark brown to brownish and colourless, mostly blocky or poorly vesicular, often slightly altered on their external parts (De Astis et al., 1997; De Rosa et al., 2016). The rest of the BT juvenile components (5–35%) are crystals (clinopyroxene and minor plagioclase, K-feldspar, olivine and amphibole) that are presents as loose fragments or rimmed by glass, with local abundance of mm-size clinopyroxene crystals. Lithic fragments are subordinate in the BT as components of the coarse ash fraction, for a total lithic content usually lower than 5 vol.% (De Astis et al., 1997; Lucchi et al., 2008; De Rosa et al., 2016), except for higher amounts up to 10% in some outcrops of the UBT on Vulcano (De Astis et al., 1997). Diffused dark (to yellowish) scoria lapilli are recognised in different stratigraphic levels of the BT on Vulcano and Lipari (Meschiari et al., 2020).

In carrying out the componentry analyses, we attributed most of the glass fragments and crystals recognised in the fine to coarse ash fractions to the juvenile BT sub-population, along with the (undifferentiated) very fine ash. Loose crystals are considered as components of the BT sub-population, because they lack in the units interlayered to the BT succession. Lithics are kept aside from this analysis because it is not possible to establish which sub-population they belong to. The

362 analysed samples contain variable amounts of exotic components that are correlated to the
363 pyroclastic deposits underlying each of the BT depositional units. These are classified here as
364 'external components' with respect to the BT sub-population. Specifically, whitish to (minor) grey
365 pumice, and obsidian fragments are recognised in the mixing band at the base of depositional unit
366 BT9 (outcrop L2) and they are fully consistent with the componentry of the underlying Falcone
367 tephra (Gioncada et al., 2005; Forni et al., 2013). Poorly vesicular, highly porphyritic dark scoria
368 and highly vesicular (sub-aphyric) white pumice are reported in the mixing band at the base of
369 deposition unit BT11 in the outcrop L12, as the main components of the underlying bed of the
370 Lower Pollara Tuffs from Salina Island (Morche, 1988; Crisci et al., 1991; Calanchi et al., 1993;
371 Lucchi et al., 2008; Forni et al., 2013). Then, the base of depositional unit BT12 sampled in the
372 outcrops L5, L10 and L12 contain highly vesicular, white (Kf-bearing) pumice, dense to moderately
373 vesicular grey pumice and banded pumice, and variable amounts of obsidian fragments and lithic
374 clasts that are the typical components of the underlying Monte Guardia pyroclastic deposits (De
375 Rosa et al., 2003). A certain amount of sub-aphyric, dark scoria ash fragments are recognised in the
376 depositional units BT9 and BT12 (in outcrops L2, L5 and L10), and they are not present in the
377 underlying Falcone and Monte Guardia units. These scoria fragments are thus included in the
378 componentry of the BT depositional units, in agreement with the report of diffused dark scoria
379 lapilli in different BT outcrops on Vulcano and Lipari (Meschiari et al., 2020). In all the analysed
380 BT depositional units the exotic components are prevalent in the lapilli and block/bombs fractions
381 (Fig. 6), and they have a polymodal grain-size distribution. Glass fragments, crystals and scoria
382 referred to the BT are instead mainly represented in the fine ash fraction. There is not a significant
383 variation of the relative abundance of exotic components with distance from the source area, as
384 evident comparing the grain-size distributions of the BT12 depositional unit in the outcrops L5, L10
385 and L12 (Fig. 6), at distances from 10 to 14.5 km from the source. However, different quantities of
386 the single grain-size classes and variations of the content of the individual exotic components are
387 reported in these outcrops as a function of the variable lithological features of the underlying Monte

Guardia unit in proximal to distal reaches, relatively to the eruptive vent in southern Lipari. Significant vertical variations of the grain-size parameters are reported for data from different levels of the same BT depositional unit. Specifically, BT12 in the L5 outcrop and BT11 in outcrop L12 were sampled at two stratigraphic levels (Fig. 6), and component analyses show an upward decrease of the content of exotic components, along with an increase in the amount of fine ash.

The analysed sub-populations of the BT, largely devoid of exotic clasts, have all fairly regular and unimodal grain-size distributions, with generally good to moderate sorting (σ_ϕ ranging between 1.29 and 2.07) and Md_ϕ ranging between 3.13 and 4.97 (Fig. 6). These values are roughly consistent with the pattern obtained by De Astis et al. (1997) for the UBT on Vulcano which defines a trend of regularly decreasing median and better sorting from proximal (σ_ϕ=0.8-1.8 and Md_ϕ=1.7-2.5 at distances of 1.5-2.0 km) to more distal locations (σ_ϕ=1.0-1.2 and Md_ϕ=3.0-3.5 at distances of 4.0-4.5 km) from the source. However, not all BT samples on Lipari fit this trend perfectly, as shown for example by the median value of 1.98 for the LIP02/17 sample in central Lipari and the moderate sorting of some samples in different sectors of Lipari. On this, we argue that the data for the BT sub-populations may be not totally depurated from the presence of external components related to the embedded lapilli and ash from the underlying units.

We also calculated the Sauter mean diameter (Sauter 1926) of the different grain size distributions (Table 3). The Sauter mean diameter is a length-scale parameter useful in characterizing fluidization processes in granular materials (Kowalczuk et al., 2016), because it defines the area-weighted mean particle size, which is important to estimate the drag applied onto particle surfaces. Because our BT sub-populations are mostly unimodal and Gaussian like, we used the method of Breard et al. (2019):

$$D_{32}(mm) = 2^{-[\mu_\varphi + \frac{ln2}{2}\sigma_\varphi^2]} \quad (1)$$

where μ_ϕ is the mean of the grain size distribution and σ_ϕ is the sorting. The values of the Sauter mean diameter of BT sub-populations range from 0.22 mm to 0.03 mm (Table 3), which results in a minimum permeability in the order of 10^{-10} – 10^{-12} m^2 (Breard et al., 2019).

4.3. Geochemical components of the mixing bands of the BT

A number of the BT depositional units investigated on both Lipari and Vulcano islands contain minor populations of exotic volcanic glass compositions that mostly plot well outside the dominant K-series compositional field of the BT, which ranges from basaltic trachy-andesites and trachy-andesites through to tephri-phonolites and trachytes. The exotic glass compositions are here named 'secondary components' consistent with Meschiari et al. (2020) (Fig. 7A, B). These secondary components are generally reported from the basal portions of the individual BT depositional units, characterised by mixing bands with the underlying pyroclastic deposits (lithofacies mA), and chemically similar to these deposits. Figure 7 provides clear evidence of the geochemical correspondence between the secondary components identified within depositional units belonging to the LBT, IBT, IBT-upper and UBT macro-units and the underlying pyroclastic units sourced from eruptions on Salina (Grey Porri Tuffs), Lipari (Punta del Perciato, Falcone, Lip1, Monte Guardia, Vallone del Gabellotto) and Vulcano (Cugni di Molinello), following the reconstructed stratigraphic succession (Fig. 2). Major and minor element glass analyses of representative samples relative to different BT depositional units and their secondary components are reported in the Supplementary File 2.

Among the analysed samples there is only one apparent lack of geochemical agreement between a BT secondary component and the underlying deposits. Specifically, the BT8 depositional unit (sample bt12/16), belonging to the IBT, directly rests above the Punta del Perciato pumice and ash in the L2 outcrop of Lipari. While it contains secondary rhyolitic glasses that are compositionally similar at a major element level to the Punta del Perciato glasses, some of these secondary glasses exhibit significantly higher K_2O and lower Na_2O contents relative to the Punta

del Perciato glasses (Figs. 7C, D, E). These offsets could reflect compositional variability in the underlying Punta del Perciato tephra unit which may have been previously undetected, considering that its previous chemical characterisation targeted only the pumice component (Albert et al., 2017). An alternative explanation is that hydration has resulted in alkali exchange within these particular glass fragments. This is apparently supported by previous IBT investigations by De Rosa et al. (2016) who identified physical evidence of fluid induced alteration (hydration) of the juvenile glass particles relating to the sin-eruptive interaction of magma and hot fluids or seawater. Indeed, our attempt to chemically analyse juvenile glass components of BT8 was entirely precluded by the significant alteration of the dominant glass component.

It is noteworthy that in some cases secondary components are also reported in BT depositional units where mixing with underlying pyroclastic deposits is not visible at a macroscopic scale. In south Lipari (outcrop L2) we sampled the IBT (sample bt14/16) that rests above the Falcone pumice succession, which are commonly subdivided into the depositional units BT9 and BT10 by the interlayered Lip1 tephra unit (Fig. 2). The sample bt14/16 contains HKCA rhyolitic secondary glass components that are broadly consistent with the Lip 1 ash (Figs. 7C, D, E), although this tephra layer is not visible in the investigated outcrop. A possible correlation of the HKCA rhyolitic secondary glass components found in bt14/16 with the underlying Falcone pumice unit is considered not probable because this sample was taken close to the base of the (overlying) Lower Pollara Tuffs, at about 2 meters above the contact with the Falcone unit. A similar situation is noticed at the Punta della Crapazza outcrop (L0) in the IBT sampled above the Falcone domes (samples LIP15/18, LIP16/18). In these samples we do observe HKCA rhyolitic secondary glasses which are chemically consistent with the Lip1 tephra layer (Figs. 7C, D, E), although the latter is not visible in the investigated stratigraphic succession. A correlation of these secondary components with the Falcone unit, which could be chemically possible, is considered unreasonable because the sampled IBT rests above the thick lava domes erupted after the Falcone pumice succession. Finally, at the outcrop of Monterosa (L7) we sampled the IBT (sample LIP45/17) above the Ischia Tephra,

and none of the interbedded stratigraphic markers from southern Lipari are visible (e.g., the Punta di Perciato, Falcone and Lip1). However, in sample LIP45/17 we do find chemical evidence of secondary HKCA rhyolitic glass components that could be attributed to any of the above-mentioned tephra units (Figs. 7C, D, E).

5. DISCUSSION

In the following, we will discuss the evidence of an origin of the BT deposits on the islands of Vulcano and Lipari from PDCs, and their specific transport and depositional mechanisms. We will not include in this discussion the BT deposits cropping out on other islands of the Aeolian archipelago or in the Sicily mainland, which do not have the same characteristics of lithofacies indicative of a PDC deposition. On this, we rely on the previous interpretation that the BT recognized further distally from the La Fossa Caldera source in the other islands of the Aeolian archipelago and Capo Milazzo in Sicily reflect fallout processes from a pulsating eruption column or co-ignimbrite ash clouds (Lucchi et al., 2008), whilst distal ash layers are recorded in Tyrrhenian and Adriatic Sea marine cores (Meschiari et al., 2020). This reflects the high mobility of fine ash in the atmosphere, which can be dispersed by both high and low atmosphere dynamics due to their long settling times (Sulpizio et al., 2008b; 2013; Giaccio et al., 2008).

5.1. Model for deposition from the BT PDCs

PDC deposits record processes occurring in the flow boundary zone, which includes the lowermost part of the current interacting with the forming deposits or with the topography (Branney and Kokelaar, 2002). Most PDC deposits originated from stratified flows in which the segregation of the particles with higher terminal velocities in the lowermost part can result in the development of a high concentration zone (Valentine, 1987; Branney and Kokelaar, 2002; Dellino et al., 2004; Sulpizio et al., 2014). This basal portion of the flow can move downslope developing different

491 depositional regimes, which can span from traction- to granular flow-dominated (see Branney and
492 Kokelaar, 2002; Sulpizio et al., 2014; Lube et al., 2021; for a review of internal structures and
493 processes). In polydisperse mixtures, including a wide range of sizes (from ash to blocks) and
494 componentry (lithics, pumice, crystals), sedimentary structures may help in deciphering the
495 depositional regime at time of deposition, defining the lithofacies of the deposit. As an example,
496 sedimentary structures like parallel to cross stratification and dune-bedding are indicative of
497 traction-dominated depositional regime from a flow-boundary zone of a diluted PDC (e.g., Andrews
498 and Manga, 2012; Doulliet et al., 2019). At the other end of PDC spectrum, reverse grading of
499 coarse clasts may indicate a granular flow-dominated depositional regime in a concentrated PDC, in
500 which grain interaction can induce kinetic sieving and kinematic squeezing of the largest particles
501 (e.g., Felix and Thomas, 2004). If the porosity within the flow-boundary zone is sufficiently low to
502 maintain the gas entrapped in the mixture, a fluid escape-dominated depositional regime may
503 develop, with deposits that appears massive and poorly sorted. Well selected, ash dominated
504 deposits are generally interpreted as gentle settling of fine-grained particles from a diluted cloud,
505 defining a direct fallout regime.

506 These sedimentological hints are of little significance to interpret the features of PDCs formed
507 only by well selected ash particles, as in the case of most of the BT deposits (Figs. 3-5). This is
508 because of the impossibility to develop sedimentary structures from very fine grain-sizes (Dellino et
509 al., 2019), which makes difficult to interpret the depositional regimes of ash-rich PDCs from
510 lithofacies analysis. This is one of the reasons why it is complicated to decipher the transport and
511 depositional mechanisms of the PDCs of the BT eruptions, which were previously generically
512 interpreted as mostly dilute PDCs or fallout from co-ignimbrite ash clouds or accompanying
513 eruption columns (De Astis et al., 1997; Lucchi et al., 2008).

514 Most of the information on the depositional mechanisms of the BT presented here is derived
515 from distinctive lithofacies mA, psA and xsA (Table 2) recognised in the proximal outcrops of the
516 UBT macro-unit on Vulcano island (outcrops V1-V4; Fig. 1A). Massive deposits of the lithofacies

517 mA are interpreted as the result of the deposition from slow-moving, ground-hugging ash-rich
518 PDCs, and their homogeneous appearance is indicative of fluid escape or granular flow depositional
519 regimes from a fine-grained, concentrated flow-boundary zone. The abundant ash aggregates
520 present in these deposits at the microscopic scale (Lucchi et al., 2008) indicate the occurrence of
521 steam in the ash cloud or fine ash aggregation driven by electrostatic force during the gentle settling
522 of ash from the more diluted portions (or the phoenix cloud) of the PDCs. Lithofacies psA and xsA
523 instead indicate grain by grain deposition from dilute and turbulent PDCs, mainly formed by coarse
524 and fine ash, in which suspension and traction are the main transport (and depositional)
525 mechanisms. Notably, in the UBT deposits investigated here, the most common is lithofacies
526 altpsmA (Fig. 3; Table 2). This is a combination of lithofacies mA and lithofacies psA, and is
527 indicative of a stepwise, repetitive aggradation of discrete PDC pulses developed within each
528 depositional unit of the BT. Massive beds are deposited from granular- or fluid-escape dominated
529 depositional regimes of concentrated PDCs and alternate with stratified ash from the turbulent and
530 diluted ash cloud accompanying the underflow during the waning stage of each pulse. This
531 depositional behaviour is consistent with the long-lasting, pulsating eruptive activity that is assumed
532 to have characterised the emplacement of the UBT macro-unit (and the rest of the BT) on Vulcano
533 island (Lucchi et al., 2008, 2013b).

534 However, intermittently stratified ash deposits of the lithofacies isA (Fig. 3) are the most
535 prominent on Vulcano island and characterise most of the BT outcrops on Il Piano area. This
536 lithofacies is not interpreted as a primary feature acquired at time of deposition of the PDCs during
537 the BT eruptions, but as the result of pervasive post-depositional disruption of the primary deposits
538 of lithofacies altpsmA. The disruption of stratified beds here is explained as due to fluid escape
539 related to dissipation of pore pressure from the underlying massive beds occurred during or
540 immediately after the emplacement of the individual beds (Fig. 8). This mechanism of fluid
541 expulsion resembles that largely described in marine and fluvial sedimentary environments (Allen,
542 1977; Owen, 1987; Selker, 1993; Owen, 1996; Odonne et al., 2011), and even in pyroclastic

543 deposits (Douillet et al., 2015). Experiments have demonstrated that fluid expulsion structures can
544 be produced by an unstable fluidization behaviour where a lower base layer of granular material is
545 inhibited from releasing intergranular fluids by the presence of an overlying low porosity top layer
546 (Nichols et al., 1994). The weight of the overlying material is balanced by an increased fluid
547 pressure in the basal layer. If the load exceeds a critical threshold, a fluid-filled crack forms and, as
548 it grows, instability causes the top layer to bend (Fig. 3G). Rupture occurs at the apex of fluid crack,
549 allowing the underlying fluid and fluidized material to burst out through the top layer. The fluidized
550 base layer material then flows through the rupture until the fluid overpressure is fully dissipated.
551 The top layer material is bent upwards around the rupture (Figs. 3E, G, H), and the resulting pillar-
552 type escape structure is preserved (Figs. 3G, H). The vigour of the burst out is greatest when the
553 base layer material has a grain-size 15% of the top layer material (Nichols et al., 1994), as in the
554 case of the BT investigated here that are composed of coarse to fine ash deposits. If the base layer
555 grain-size is less than 8% of the top layer then base layer material will pass through the top layer
556 pore spaces, without forming an escape structure. Depending on how much the disruption
557 mechanism was pervasive, the BT deposits in the investigated outcrops have either largely
558 preserved the original lithofacies (Fig. 3F) or they are almost entirely massive with only fragments
559 of laminae distributed unevenly as relicts of the original stratified lithofacies (Fig. 3I). It is therefore
560 important to note that in many cases the massive deposits of the BT on Vulcano are not a primary
561 lithofacies, but they are instead the result of pervasive post-depositional fluid escape processes
562 occurred during or immediately after their emplacement. De Astis et al. (1997) suggested that the
563 fragments of stratified ash embedded in some massive BT deposits was due to fragmentation of a
564 stratified layer due to an external trigger (earthquakes), with subsequent sinking of the denser and
565 heavier fragments into the soft massive deposits. We consider this explanation less probable
566 because the evidence of disrupted stratification and fragments of stratified ash is recognised in a
567 number of BT depositional units at different stratigraphic levels, which makes it difficult to assume
568 a repetitive trigger external to the depositional system. Moreover, the upward bending of the

569 fragmentation points and pillar-type structures observed in the lithofacies isA are more consistent
570 with a model of fluid escape. Small ash diapirs were explained by De Astis et al. (1997) as a result
571 of a significant amount of (liquid) water in the massive deposits, but we consider more probable a
572 process of fluid escape due to dissipation of the pore pressure during deposition of the BT and
573 subsequent compaction.

574 Most of the BT outcrops on Lipari and southern Vulcano are characterised by homogeneously
575 massive lithofacies that are referred to deposition from PDCs on the base of significant thickness
576 variations as function of paleo-topography of the individual BT depositional units, which is not fully
577 consistent with primary fallout processes (Lucchi et al., 2008). Progressive aggradation of different
578 PDC pulses can be argued from faint banding due to colour differences or subtle grain-size variations
579 within massive deposits. Also, in this case the deposits are mostly formed by ash, which raises the
580 issue if they were erupted as mixtures of fine particles or if the coarse particles were deposited in very
581 proximal areas. It was suggested that an efficient hydromagmatic fragmentation have produced a
582 large amount of fine ash with respect to lapilli and blocks. Evidence that fragmentation was driven
583 mostly by magma-water interaction is provided by SEM results showing that equant blocky
584 fragments, with quenching cracks and abundant adhering particles are dominant in the BT deposits
585 (De Astis et al., 1997; Lucchi et al., 2008). This is consistent with a location of eruptive vents inside
586 the La Fossa Caldera, the floor of which might have been below or near sea level during most of its
587 evolution starting from c. 80 ka (De Astis et al., 2013). Another possible explanation, which may be
588 concomitant with efficient hydromagmatic fragmentation, is that coarse-grained material has been
589 probably deposited in the caldera depression, which is now filled and completely covered with the
590 more recent deposits of La Fossa cone (De Astis et al., 1997; Lucchi et al., 2008). For the deposits
591 outcropping on Vulcano island, it must be considered that decoupling of basal (coarse-grained) and
592 upper (fine-grained) parts of the PDCs has occurred when the PDCs impacted against the caldera
593 walls (Fig. 8), with only the finer grained parts transported by turbulence in the ash clouds able to
594 overpass the topographic obstacle and spread over the central and southern parts of Vulcano island.

595 The massive BT deposits can be interpreted either as the result of direct fallout-dominated flow-
596 boundary zones or fluid-escape (or even granular flow) depositional regimes in well sorted, ash-
597 dominated pyroclastic mixtures (cf. Branney and Kokelaar, 2002; Sulpizio et al., 2007; 2010). Direct
598 fallout implies mainly vertical gentle settling of particles in a slow moving or motionless pyroclastic
599 cloud, whilst deposition from granular flow or fluid-escape dominated flow-boundary zones implies
600 lateral movement of the moving flow. The key feature for establishing a depositional mechanism
601 from laterally spreading PDCs is the evidence at the base of the BT depositional units of mixing bands
602 containing a substantial component of ash and lapilli made up of pumice, scoria and lithics from the
603 underlying pyroclastic deposits (lithofacies mixAL; Fig. 4). These mixing bands indicate erosion and
604 incorporation of loose material from the underlying beds into the moving ash flows that deposited the
605 BT. The general poor sorting and massive appearance of the mixed deposits are suggestive of
606 sedimentation from a current in which the rate of supply (Rs) is higher than the rate of deposition
607 (Rd), which induces rapid development of a highly concentrated zone above the flow boundary,
608 dominated by a granular flow (or fluid-escape) depositional regime. The moving flows relative to the
609 BT exerted shear stress over the loose, erodible pyroclastic deposits that represented their substratum,
610 causing entrapment of exotic clasts into the flow body (Fig. 9). The reverse grading of entrained
611 coarse clasts observed in some places (e.g. Fig. 4E) suggests that a lateral movement under high shear
612 occurred during transportation and deposition of the BT PDCs. Such reverse grading of coarse clasts
613 is attributed to dispersive pressure processes induced by grain-grain collision in a high-concentration
614 zone at the base of the current (Lowe,1982; Sohn,1997; Dellino et al., 2004).
615 Clast embedding at the base of BT deposits was previously signalled by Lucchi et al. (2008)
616 only in the outcrops of southern Lipari and Gelso (south Vulcano; Fig. 1A), whilst here we document
617 the occurrence of entrainment processes across the entire study area, from northern Lipari to central
618 and southern Vulcano, thus substantially enlarging the area where there is evidence of substrate
619 erosion exerted by the BT PDCs. The mixing bands are easily recognised in the field where the
620 eroded/remobilized bed is made of lapilli (due to the contrasting grain-size) or light-coloured clasts

(due to contrasting colour), as also supported by grain size and component analyses of selected base layers of BT depositional units (Fig. 6). When the mixing material is not visible at visual inspection, it can be documented by secondary glass components plotting outside of the main compositional field of the BT (Fig. 7). As an example, the rhyolitic Lip1 (ash) tephra layer from an eruptive vent in southern Lipari is characterised by a very discontinuous areal distribution. This can be due to processes of wind-reworking or post-depositional erosion, as typically occurs for ash beds, but the role played by processes of erosion and clast incorporation by the BT currents is clearly outlined by the finding of secondary components chemically correlated to Lip1 within the BT depositional unit above (Fig. 7C-E), even where there is no direct evidence of the Lip1 tephra layer in the field.

Overall, sedimentological analyses, combined with grain-size, componentry and geochemical investigation, provide unequivocal evidence that the BT were deposited from PDCs laterally spreading from the La Fossa caldera all over the islands of Lipari and Vulcano. De Rosa et al. (2016) suggested that mixing bands are the result of post-eruptive remobilization of the BT deposits on pre-existing steep slopes. The occurrence of mixing bands even on flat topography make us confident in excluding reworking as a primary mechanism. Notably, the evidence of mixing bands at the base of distinct BT depositional units even in the northern sector of the island of Lipari enlarges the area where the PDCs that deposited the BT had a potential of eroding the substratum and embedding clasts from the underlying units up to distances of 16-17 km from the source area, therefore substantially increasing the estimate of the maximum run-out of currents of this type. This is coherent with experimental models (Girolami et al. 2008; Roche et al. 2008; Cagnoli and Romano 2010; Dellino et al. 2019) showing that PDCs transporting mostly fine ash, like those of the BT on Lipari, may travel further and possess a higher capacity of impact over the territory with respect to those characterised by coarser material. On this, the calculated values of Sauter median diameters (Table 3) indicate very low porosity of the BT pyroclastic mixture in the flow boundary zone (in the order of 10^{-10}–10^{-12} m^2), which suggests long time retention of gas within the mixture enhancing fluidization and flow mobility (Druitt et al. 2007; Smith et al., 2018; Lube et al. 2019; Roche et al., 2021).

It cannot be excluded that a significant part of proximal to medial massive BT deposits on Vulcano and Lipari, where evidences of shear structures or exotic component mixing are absent, is the result of ash fallout from co-ignimbrite ash clouds or eruption columns, a process that is suggested to be dominant in the more distal outcrops in the other islands of the Aeolian archipelago and the Capo Milazzo peninsula. Given the cryptic nature of the BT deposits where the contacts between different depositional units cannot be easily recognised, the volume fraction of the ash deposits possibly deposited from fallout processes could not be discerned. This does not weaken the evidence from sedimentological characteristics, which indicates a dominant deposition of the BT on Lipari and Vulcano from ground hugging PDCs.

The fine-grained, well sorted grain size of BT deposits is unusual for PDCs deposits recognised widely and apparently crossing between adjacent islands and deserves some further consideration and discussion. It is notable that the islands of Vulcano and Lipari are currently separated by the narrow and shallow sea-water inlet of Bocche di Vulcano with a minimum depth of c. 40 m and width of less than 1 km. Considering that most of the 80-6 ka time-stratigraphic interval of the BT has elapsed in lowstand conditions (Rohling et al., 2014), this sea-water inlet might also have been for a long time narrower and shallower. This means that most of the PDCs that deposited the BT on Lipari mainland had to overcome a small sea inlet which did not actually hinder their lateral spreading but might have influenced their transport and depositional behaviour. The PDCs that passed over the sea inlet in fact had to have density lower than sea water (i.e., less than 1025 kg/m^3). This is an unrealistic density for the basal part of any PDCs, in which the density stratification induces packing of solid particles with density usually in excess of that of water. Therefore, it can be reasonably assumed that the basal, coarser and more concentrated portion of PDCs spreading from Vulcano sunk into the sea water accompanied by decoupling of the turbulent, more diluted portion of the PDCs which was able to pass over the sea and reach the Lipari mainland (Fig. 10). This water density bias and the decoupling of the basal and upper portions of the PDCs could explain the grain size characteristics of the BT deposits on Lipari island. When these PDCs reached Lipari they encountered a rugged and irregular

topography due to the presence of a rhyolitic dome complex emplaced between c. 50 and 20 ka. The flow of diluted and turbulent PDCs over variable slopes produced loss of momentum, which reflected in loss of turbulence and less capacity to maintain solid particles in suspension. This produced an increased concentration of particles in the flow boundary and transition to dominant granular flow or fluid-escape regimes at time of deposition (Fig. 10). Lithofacies analysis indicates that the BT PDCs mostly deposited in granular flow or fluid escape regimes due to interaction with the paleo-topography and increased sedimentation rate, whilst the currents travelled large distances in a dilute and turbulent behaviour reaching distances around 16-17 km from the source (up to northern Lipari). The (more) concentrated basal portions of these PDCs were generally able to erode the incoherent substratum embedding clasts from the underlying units and produced sin-depositional shear structures (see below). In any case, the distance travelled by PDCs (around 16-17 km) suggests high mass discharge rates feeding the currents spreading from the vent (Roche et al., 2021).

5.2 Physical characteristics of the PDCs inferred from shear structures

In addition to the mixed lithofacies, also the sedimentary structures of lithofacies ucAL, rfAL, ruAL recognised in outcrops of southern and central Lipari are indicative of an effective lateral transport and shear stress exerted by the ash flows of the BT over the substratum (Fig. 9).

In particular, the undulated contacts (lithofacies ucAL) between the BT depositional units and the underlying lapilli beds in outcrops L1 and L5 may be referred to conditions of high shear stress exerted by the overriding currents to the loose lapilli substratum, which induces remobilization of its upper part and formation of waves with variable wavelength and imbrication of coarser clasts. Such imbrication testifies for the occurrence of traction carpet processes, in which the static bed material is moved and reorganised in a frictional regime by the overriding flow (e.g. Sohn, 1997; Dellino et al., 2004). Recumbent flame structures (lithofacies rfAL) also indicate high shear stress exerted by the overriding PDCs of the BT eruptions over the underlying lapilli beds, which produce incorporation of lapilli that are aligned downflow and bended to form an alignment of lapilli within

699 the BT ash deposit for a distance up to some meters. Instead, the small hook-like structures of the
700 lithofacies ruAL is related to conditions of moderate shear stress exerted from the overriding ash
701 flow, which was able to rip-up lapilli from the underlying bed into the BT unit but with no
702 significant lateral displacement of the upper part of the structure. The formation of the different
703 shear structures depends on both flow and erodible deposit characteristics, like flow velocity,
704 depositional regime, perpendicular load component of the moving flow, grain packing in the
705 deposit, and terminal velocity of erodible clasts, among others. Currently, there are few laboratory
706 experiments on entrapment of loose substratum into the moving flow, carried out using synthetic
707 material (Roche et al. 2013, 2016; Roche 2015). They mainly focus on clast entrapment due to
708 underpressure at the head of the moving flow, a process different from that here described, which
709 does not produce the observed syn-depositional shear structures. In order to unravel the flow
710 conditions responsible of the various deposit characteristics and structures some hints may be
711 gained from published studies on PDC erosion based on field evidence. Following Doulliet et al.
712 (2019) and Pollock et al. (2019), the recumbent flame structures are referred to PDCs of similar
713 concentration to the undulated structures, and the latter represent an earlier phase of growth of the
714 recumbent flame structures. Moreover, the recumbent flame structures are a reliable indicator of the
715 approximate local direction of the currents. Additionally, the recumbent flame structures are related
716 to conditions of high concentration in the flow boundary zone (Pollock et al., 2019), indicating that
717 the BT were deposited by mostly concentrated PDCs.

718 By a physical point of view, the undulated (lithofacies ucAL), recumbent flame (lithofacies
719 rfAL) and rip-up structures (lithofacies ruAL) recognised at the base of BT depositional units are a
720 signature of instabilities occurring at the boundary of two sheared granular media, and they may
721 represent the frozen record of granular, pseudo-Kelvin–Helmholtz instabilities. Waves and
722 overturned stratification like those described at the base of BT are usually the result of simple shear
723 exerted by the overriding flow on the loose substratum (Allen and Banks, 1972; Mills, 1983;
724 Valentine et al., 1989; Røe and Hermansen, 2006; Douillet et al., 2015; Pollock et al., 2019). They

725 have been also described in several analogue experimental studies with granular flows over grain
726 beds (Goldfarb et al., 2002; Mangeney et al., 2010; Rowley et al., 2011; Roche et al., 2013; Farin et
727 al., 2014).
728 Shear stress τ is defined as:
729
730 $$\tau = u_*^2 \rho_{PDC} \quad (2)$$
731
732 where u∗ is the shear velocity, and ρ_{PDC} is the current density. The minimum velocity needed for
733 starting bed instability is given by:
734
735 $$u_{*min} = \left[\frac{g\lambda}{2\pi}\frac{(1-x^2)}{x}\right]^{1/2} \quad (3)$$
736
737 where *g* is the gravity acceleration, λ is the wavelength of bed instability, and *x* the relative flow
738 concentration (ρ_{PDC}/ρ_{bed}) (Doulliet et al., 2015). Eq. (3) states that the wavelength of the
739 instabilities depends on shear velocity and the ratio between particle concentrations of the PDC and
740 the underlying bed. It is interesting to note that Eq. (3) holds for $0 \leq x \leq 1$ (Douillet et al., 2015),
741 which means that instabilities can form only if particle concentration in the bed is greater than that
742 in the flow. Figure 11 shows that the more diluted the flow is (lower numbers of *x*), the more is the
743 velocity required to form bed instabilities. In all PDCs the solid-void ratio and flow density (ρ_{PDC})
744 can vary greatly with height, producing flow stratification (e.g., Valentine, 1987; Dellino et al.,
745 2004), and developing granular flow or fluid-escape dominated flow-boundary zones. The fluid and
746 solid components abundance and densities determine the physical properties of the flow, which
747 greatly depend on grain-size distributions and relative abundance of the different solid
748 componentry. Without direct measurements, a gross estimate of particle concentration and ρ_{PDC} can
749 be obtained from the deposits for granular/fluid escape-dominated flows. Assuming a characteristic

750 solid-fluid ratio of 50-60% for ash rich deposits and a mean solid density of 2400 kg m^{-3} (e.g.,
751 Sulpizio et al., 2007; Breard and Lube, 2017; Lube et al. 2019), it results a range of ρ_{PDC} of ca.
752 1100-1400 kg/m^{-3}. Considering that the solid volume fraction can reach 70% in PDC deposits (Gase
753 et al., 2018) and assuming a flow concentration of 50-60 vol.%, it results in a relative flow
754 concentration *(x)* of 10-20% lower than the deposit, which can be used to constrain the minimum
755 shear velocity to form the observed bed instabilities. For wavelength number of 0.16 (l=40 cm) the
756 minimum basal shear velocity is less than 1 m s^{-1}, while for wavelength number of 0.72 (l=450 cm)
757 it is less than 2 m s^{-1} (Fig. 11), a value comparable to that obtained for the Peach Spring ignimbrite
758 (Roche et al., 2016). It is to note that the calculated velocities do not reflect velocities at the flow
759 front, but instead reflect the basal slip velocity at the time of instability formation. The resulting
760 minimum basal shear stress, which refers the very base of the stratified current (a few mm-cm) may
761 be calculated in the range of 1-4.5 kPa using Eq. (1).
762
763 **6. CONCLUSIONS**
764
765 A sedimentological analysis of lithofacies, combined with grain-size and componentry
766 investigation and grain-specific volcanic glass compositional data, for a large number of the different
767 depositional units of the ash-rich Brown Tuffs (BT) has been carried out on Lipari and Vulcano to
768 provide constraints on their transport and depositional mechanisms and dispersal area. We rely on the
769 framework of knowledge acquired so far according to which the BT were generated over a long-time
770 interval between c. 80 and 6 ka by pulsating hydromagmatic eruptions from eruptive vent(s) inside
771 the La Fossa caldera on Vulcano. The following are the main outcomes of the present work:
772 1. The UBT on Vulcano (24-6 ka) are deposited from ground-hugging ash-rich pyroclastic
773 density currents (PDCs) that have surmounted the caldera walls. Alternating massive and
774 planar to cross stratified deposits reflect a repetitive aggradation of PDC pulses
775 characterised by either fluid escape or granular flow depositional regimes from a fine-

776 grained, concentrated flow-boundary zone (lithofacies mA) or grain by grain deposition
777 from dilute and turbulent PDCs (lithofacies psA-xsA) during the waning stage of each pulse.
778 2. Intermittently stratified ash deposits of the UBT on Vulcano, with distinctive upwards bends
779 and pillar- type escape structures through the rupture points are interpreted as the result of
780 post-depositional disruption of the primary deposits due to fluid escape related to dissipation
781 of pore pressure between layers at different porosity. This process can be pervasive to
782 produce almost entirely massive UBT deposits with only fragments of laminae distributed
783 unevenly as relicts of the original stratified lithofacies.
784 3. Most of the BT on Lipari are emplaced by PDCs that have likely travelled over a narrow
785 sea inlet. The water density bias produced decoupling of basal denser parts of the currents,
786 which sunk into the sea, from the turbulent and more diluted upper parts, able to reach
787 Lipari. This induced selection of particles and accounts for the unusual good sorting and
788 very fine grain size distribution of BT deposits on Lipari island. Topography-induced
789 decoupling occurred on Vulcano due to the interaction of southwards laterally spreading
790 PDCs with the La Fossa Caldera walls. Most of the BT on Lipari and partly on Vulcano
791 were deposited in fluid escape or granular flow regimes induced by the interaction of the
792 turbulent parent flows with the paleo-topography, which caused loss of turbulence and
793 concentration of the solid particles in the flow boundary zone.
794 4. Most of the individual BT depositional units on Lipari (and Vulcano) are characterised at
795 the base by mixing bands containing pumice, scoria and lithic clasts ripped-up and
796 embedded from the loose underlying pyroclastic units, as outlined by field study supported
797 by grain-size and component analyses and geochemical glass investigation of the different
798 components. These mixing bands indicate erosion and incorporation of loose material from
799 the underlying beds into the laterally spreading ash flows that deposited the BT. The
800 recognition of these structures up to the northern sector of Lipari indicates that the PDCs

during the BT eruptions travelled up to distances of (at least) 16-17 km from the source area and possessed a high capacity of impact over the territory.

5. Undulated, recumbent flame and rip-up structures are recognised at the base of some BT depositional units on southern and central Lipari as the result of effective lateral transport and moderate to high shear stress exerted by the ash flows of the BT to the substratum. These structures provide indications on the approximate local south-to-north direction of the currents, and the conditions of high solid concentration of the PDCs that deposited these BT. Moreover, they can be adopted to estimate a basal shear velocity of the currents of up to c. 2 m s^{-1} and a shear stress in the range of 1-4.5 kPa at the time of structure formation.

In conclusion, massive ash deposits of the BT can actually result from the spreading of PDCs that possess a high erosive power and shear strength at the flow base, representing a substantial hazard for tens of km away from the source area, which is amplified by the fine grain size that helps maintaining fluidization and increasing flow mobility.

ACKNOWLEDGEMENTS

We thank three anonymous reviewers for their thoughtful suggestions to the first draft of this manuscript, and Catherine Chagué for her kind and careful editing. Sara Meschiari was funded through a Ph.D. Scholarship of the University of Bologna-Alma Mater Studiorum. Paul G. Albert was funded through a UKRI Future Leaders Fellowship (MR/S035478/1).

REFERENCES

Albert, P.G., Tomlinson, E.L., Smith, V.C., Di Traglia, F., Pistolesi, M., Morris, A., Donato, P., De Rosa, R., Sulpizio, R., Keller, J., Rosi, M., Menzies M., 2017. Glass geochemistry of pyroclastic deposits from the Aeolian Islands in the last 50 ka: a proximal database for tephrochronology. Journal of Volcanology and Geothermal Research 336, 81-107.

827 Allen, J.R.L., 1977. The possible mechanics of convolute lamination in graded sand beds. Journal of
828 the Geological Society London 134, 19–31.
829 Allen, J.R.L., Banks, N.L., 1972. An interpretation and analysis of recumbent folded deformed cross
830 bedding. Sedimentology 19, 257-283.
831 Allen, S.R., Cas, R.A.F., 1998. Rhyolitic fallout and pyroclastic density current deposits from a
832 phreatoplinian eruption in the eastern Aegean Sea, Greece. Journal of Volcanology and
833 Geothermal Research 86, 219–251.
834 Andrews, B.J., Manga, M., 2012. Experimental study of turbulence, sedimentation, and coignimbrite
835 mass partitioning in dilute pyroclastic density currents. Journal of Volcanology and Geothermal
836 Research 225-226, 30-44.
837 Barberi, F., Gasparini, P., Innocenti, F., Ferrara, G., Villari, L., 1973. Volcanism of the southern
838 Tyrrhenian Sea and its geodynamic implications. Journal of Geophysical Research 78, 5221-
839 5232.
840 Beccaluva, L., Gabbianelli, G., Lucchini, F., Rossi, P.L., Savelli, C., 1985. Petrology and K/Ar ages
841 of volcanics dredged from the Aeolian seamounts: implications for geodynamic evolution of
842 the Southern Tyrrhenian basin. Earth and Planetary Science Letters 74, 187–208.
843 Bergeat, A., 1899. Die Äolischen Inseln (Stromboli, Panaria, Salina, Lipari, Vulcano, Filicudi und
844 Alicudi). Abhandlungen der Mathematisch-Physikalischen Klasse der Königlich Bayerischen
845 Akademie der Wissenschaften, vol. 20 I. Abt., München, 274 pp (in German)
846 Bernard, J., Kelfoun, K., Le Pennec, J.-L., Vallejo Vargas, S., 2014. Pyroclastic flow erosion and
847 bulking processes; comparing field-based vs. modeling results at Tungurahua Volcano,
848 Ecuador. Bulletin of Volcanology 76, 1-16.
849 Blott, S.J., Pye, K., 2001. GRADISTAT: a grain size distribution and statistics package for the
850 analysis of unconsolidated sediments. Earth Surface Processes and Landforms 26, 1237–
851 1248.

852 Branney, M.J., Kokelaar, P., 2002. Pyroclastic Density Currents and the Sedimentation of
853 Ignimbrites. Geological Society London Memoirs 27, 143 pp.
854 Breard, E.C.P., Lube, G., 2017. Inside pyroclastic density currents—Uncovering the enigmatic flow
855 structure and transport behaviour in large- scale experiments. Earth and Planetary Science
856 Letters 458, 22–36.
857 Breard, E.C.P., Jones, J.R., Fullard, L., Lube, G., Davies, C., Dufek, J., 2019. The permeability of
858 volcanic mixtures - Implications for pyroclastic currents. Journal of Geophysical Research,
859 Solid Earth 124. https://doi.org/10.1029/2018JB016544
860 Brosch, E., Lube, G., 2020. Spatiotemporal sediment transport and deposition processes in
861 experimental dilute pyroclastic density currents. Journal of Volcanology and Geothermal
862 Research 401, 106946. https://doi.org/10.1016/j.jvolgeores.2020.106946.
863 Cagnoli, B., Romano, G.P., 2010. Effect of grain size on mobility of dry granular flows of angular
864 rock fragments: An experimental determination. Journal of Volcanology and Geothermal
865 Research 193, 18–24.
866 Calanchi, N., De Rosa, R., Mazzuoli, R., Rossi, P.L., Santacroce, R., Ventura, G., 1993. Silicic
867 magma entering a basaltic magma chamber: eruptive dynamics and magma mixing – an
868 example from Salina (Aeolian Islands, southern Tyrrhenian Sea). Bulletin of Volcanology 55,
869 504–522.
870 Cas, R.A.F., Wright, J.V., 1987. Volcanic Successions. Unwin Hyman, London, 528 pp.
871 Cas, R.A.F., Wright, H.M.N., Folkes, C.B., Lesti, C., Porreca, M., Giordano, G., Viramonte, J.G.,
872 2011. The flow dynamics of an extremely large volume pyroclastic flow, the 2.08-Ma Cerro
873 Galán Ignimbrite, NW Argentina, and comparison with other flow types. Bulletin of
874 Volcanology 73, 1583–1609.
875 Carey, S.N., 1991. Transport and deposition of tephra by pyroclastic flows and surges. SEPM, Society
876 for Sedimentary Geology, Special Publications 45, 39–57.
877 Chappell, J., Shackleton, N.J., 1986. Oxygen isotopes and sea level. Nature 324, 137–140.

878 Chiarabba, C., De Gori, P., Speranza, F., 2008. The Southern Tyrrhenian Subduction Zone: deep
879 geometry, magmatism and Plio-Pleistocene evolution. Earth and Planetary Science Letters 268,
880 408–423.
881 Chough, S.K., Sohn, Y.K., 1990. Depositional mechanics and sequences of base surges, Songaksan
882 tuff ring, Cheju Island, Korea. Sedimentology 37, 1115–1135.
883 Cicchino, A., Zanella, E., De Astis, G., Lanza, R., Lucchi, F., Tranne, C.A., Airoldi, G., Mana S.,
884 2011. Rock magnetism and compositional investigation of Brown Tuffs deposits at Lipari and
885 Vulcano (Aeolian Islands – Italy). Journal of Volcanology and Geothermal Research 208, 23-
886 28.
887 Cole, P.D., Guest, J.E., Duncan, A.M., 1993. The emplacement of intermediate volume ignimbrite: a
888 case study from Roccamonfina volcano, southern Italy. Bulletin of Volcanology 55, 467–480.
889 Colella, A., Hiscott, R.N., 1997. Pyroclastic surges of the Pleistocene Monte Guardia sequence
890 (Lipari Island, Italy): depositional processes. Sedimentology 44, 47–66.
891 Crisci, G.M., De Rosa, R., Lanzafame, G., Mazzuoli, R., Sheridan, M.F., Zuffa, G.G., 1981. Monte
892 Guardia Sequence: a Late-Pleistocene Eruptive Cycle on Lipari (Italy). Bulletin of Volcanology
893 44, 241-255.
894 Crisci, G.M., Delibrias, G., De Rosa, R., Mazzuoli, R., Sheridan, M.F., 1983. Age and petrology of
895 the Late-Pleistocene Brown Tuffs on Lipari, Italy. Bulletin of Volcanology 46, 381-391.
896 Crisci, G.M., De Rosa, R., Esperanca, S., Mazzuoli, R., Sonnino, M., 1991. Temporal evolution of a
897 three component system: the island of Lipari (Aeolian Arc, southern Italy). Bulletin of
898 Volcanology 53, 207-221.
899 De Astis, G., Dellino, P., De Rosa, R., La Volpe, L., 1997. Eruptive emplacement mechanism of fine
900 grained pyroclastic deposits widespread on Vulcano Island. Bulletin of Volcanology 59, 87-
901 102.

De Astis, G., Ventura, G., Vilardo, G., 2003. Geodynamic significance of the Aeolian volcanism (Southern Tyrrhenian Sea, Italy) in light of structural, seismological and geochemical data. Tectonics 22, 1040–1057.

De Astis, G., Lucchi, F., Dellino, P., La Volpe, L., Tranne, C.A., Frezzotti, M.L., Peccerillo, A., 2013. Geology, volcanic history and petrology of Vulcano (central Aeolian archipelago). Geological Society London, Memoirs 37, 281–348.

De Rosa, R., Donato, P., Gioncada, A., Masetti, M., Santacroce, R. 2003. The Monte Guardia eruption (Lipari, Aeolian Islands): an example of a reversely zoned magma mixing sequence. Bulletin of Volcanology 65, 530–543.

De Rosa, R., Donato, P., Scarciglia, F., 2016. On the origin and post-depositional history of widespread massive ash deposits: the case of Intermediate Brown Tuffs (IBT) of Lipari (Aeolian Islands, Italy). Journal of Volcanology and Geothermal Research 327, 135-151.

Dellino, P., Isaia, R., Veneruso, M., 2004. Turbulent boundary layer shear flows as an approximation of base surge at Campi Flegrei (Southern Italy). Journal of Volcanology and Geothermal Research 133, 211–228.

Dellino, P., Zimanowski, B., Buttner, R., La Volpe, L., Mele, D., Sulpizio, R., 2007. Large-scale experiments on the mechanics of pyroclastic flow: design, engineering, and first results. Journal of Geophysical Research 112, B04202. https://doi.org/10.1029/2006JB004313.

Dellino, P., Buttner, R., Dioguardi, F., Doronzo, D.M., La Volpe, L., Mele, D., Sonder, I., Sulpizio, R., Zimanowski, B., 2010. Experimental evidence links volcanic particle characteristics to pyroclastic flow hazard. Earth and Planetary Science Letters 295, 314–320.

Dellino, P., De Astis, G., La Volpe, L., Mele, D., Sulpizio, R., 2011. Quantitative hazard assessment of phreatomagmatic eruptions at Vulcano (Aeolian Islands, Southern Italy), as obtained by combining stratigraphy, event statistics and physical modelling. Journal of Volcanology and Geothermal Research 201, 264-384.

927 Dellino, P., Dioguardi, F., Doronzo, D.M., Mele, D., 2019. The rate of sedimentation from turbulent
928 suspension: An experimental model with application to pyroclastic density currents and
929 discussion on the grain-size dependence of flow runout. Sedimentology 66, 129–145.
930 Douillet, G.A., Taisne, B., Tsang-Hin-Sun, M.S.K., Kueppers, U., Dingwell, D.B., 2015. Syn-
931 eruptive, soft-sediment deformation of deposits from dilute pyroclastic density current: triggers
932 from granular shear, dynamic pore pressure, ballistic impacts and shock waves. Solid Earth 6,
933 553-572.
934 Douillet, G.A., Bernard, B., Bouysson, M., Chaffaut, Q., Dingwell, D.B., Gegg, L., Hoelscher, I.,
935 Kueppers, U., Mato, C., Ariane Ritz, V., Schlunegger, F., Witting, P., 2019. Pyroclastic dune
936 bedforms: macroscale structures and lateral variations. Examples from the 2006 pyroclastic
937 currents at Tungurahua (Ecuador). Sedimentology 66, 1531-1559.
938 Druitt, T.H., 1998. Pyroclastic density currents. Geological Society London, Special Publications
939 145, 145–182.
940 Druitt, T.H., Avard, G., Bruni, G., Lettieri, P., Maez, F., 2007. Gas retention in fine-grained
941 pyroclastic flow materials at high temperatures. Bulletin of Volcanology 69, 881-901.
942 Dufek, J., Esposti Ongaro, T., Roche, O., 2015. Pyroclastic density currents: processes and models.
943 In: Sigurdsson, H., Houghton, B., McNutt, S., Rymer, H., Stix, J. (Eds.), The Encyclopedia of
944 Volcanoes (second edition). Academic Press, Elsevier, pp. 631–648.
945 Ellam, R.M., Menzies, M.A., Hawkesworth, C.J., Leeman, W.P., Rosi, M., Serri, G., 1988. The
946 transition from calc-alkaline to potassic orogenic magmatism in the Aeolian Islands, Southern
947 Italy. Bulletin of Volcanology 50, 386–398.
948 Farin, M., Mangeney, A., Roche, O., 2014. Fundamental changes of granular flow dynamics,
949 deposition, and erosion processes at high slope angles: insights from laboratory experiments.
950 Journal of Geophysical Research-Earth 119, 504–532.

951 Félix, G., Thomas, N., 2004. Relation between dry granular flow regimes and morphology of
952 deposits: Formation of levées in pyroclastic deposits. Earth Planetary and Science Letters 221,
953 197-213.
954 Folk RL, Ward WC., 1957. Brazos River bar: a study in the significance of grain size parameters.
955 Journal of Sedimentary Petrology 27, 3–26.
956 Forni, F., Lucchi, F., Peccerillo, A., Tranne, C.A., Rossi, P.L., Frezzotti, M.L., 2013. Stratigraphic
957 and geological evolution of the Lipari volcanic complex (central Aeolian archipelago).
958 Geological Society London Memoirs 37, 213-279.
959 Francalanci, L., Taylor, S.R., Mcculloch, M.T., Woolhead, J.D., 1993. Geochemical and isotopic
960 variations in the calc-alkaline rocks of Aeolian arc, southern Tyrrhenian Sea, Italy: constraints
961 on magma genesis. Contributions to Mineralogy and Petrology 113, 300–313.
962 Francalanci, L., Lucchi, F., Keller, J., De Astis, G., Tranne, C.A., 2013. Eruptive, volcano-tectonic
963 and magmatic history of the Stromboli volcano (north-eastern Aeolian archipelago). Geological
964 Society London Memoirs 37, 395–469.Freundt, A., Schmincke, H.U., 1986. Emplacement of
965 small-volume pyroclastic flows at Lacher See (East Eifel, Germany). Bulletin of Volcanology
966 48, 39–59.
967 Gase, A., Bradford, J.H., Brand, B., 2018. Estimation of porosity and water saturation in dual porosity
968 pyroclastic deposits from joint analysis of compression, shear, and electromagnetic velocities.
969 Geophysics 83, 1-39.
970 Giaccio, B., Isaia, R., Fedele, F.G., Di Canzio, E., Hoffecker, J., Ronchitelli, A., Sinitsyn, A.A.,
971 Anikovich, M., Lisitsyn, S.N., Popov, V.V., 2008. The Campanian Ignimbrite and Codola
972 tephra layers: Two temporal/stratigraphic markers for the Early Upper Palaeolithic in southern
973 Italy and eastern Europe. Journal of Volcanology and Geothermal Research 177, 208–226.
974 Gioncada, A., Mazzuoli, R., Bisson, M., Pareschi, M.T., 2003. Petrology of volcanic products
975 younger than 42 ka on the Lipari-Vulcano complex (Aeolian Islands, Italy): an example of

volcanism controlled by tectonics. Journal of Volcanology and Geothermal Research 122, 191–220.

Gioncada, A., Mazzuoli, R., Milton, A.J., 2005. Magma mixing at Lipari (Aeolian Islands, Italy): insights from textural and compositional features of phenocrysts. Journal of Volcanology and Geothermal Research 145, 97–118.

Girolami, L., Druitt, T.H., Roche, O., Khrabrykh, Z., 2008. Propagation and hindered settling of laboratory ash flows. Journal of Geophysical Research 113, B02202. http://dx.doi.org/10.1029/2007JB005074.

Goldfarb, D.J., Glasser, B.J., Shinbrot, T., 2002. Shear instabilities in granular flows. Nature 415, 302–305.

Gurioli, L., Cioni, R., Sbrana, A., Zanella, E., 2002. Transport and deposition of pyroclastic density currents over an inhabited area: the deposits of the AD 79 eruption of Vesuvius at Herculaneum, Italy. Sedimentology 49, 1–26.

Hornig-Kjarsgaard, I., Keller, J., Koberski, U., Stadlbauer, E., Francalanci, L., Lenhart, R., 1993. Geology, stratigraphy and volcanological evolution of the island of Stromboli, Aeolian arc, Italy. Acta Vulcanologica 3, 21–68.

Keller, J., 1967. Alter und Abfolge der vulkanischen Ereignisse auf den Aolischen Inseln. Berichte der Naturforschenden Gesellschaft zu Freiburg i. Br. 57, 33–67 (in German).

Keller, J., 1980a. The island of Salina. Rendiconti della Società Italiana di Mineralogia e Petrologia 36, 489-524.

Keller, J., 1980b. The Island of Vulcano. Rendiconti della Società Italiana di Mineralogia e Petrologia 36, 369-414.

Keller, J., Ryan, W.B.F., Ninkovich, D., Altherr, R., 1978. Explosive volcanic activity in the Mediterranean over the past 200 000 yr as recorded in deep-sea sediments. Geological Society of America Bulletin 89, 591–604.

LaBerge, R.D., Giordano, G., Cas, R.A.F., Ailleres, L., 2006. Syn-depositional substrate deformation produced by the shear force of a pyroclastic density current: An example from the Pleistocene ignimbrite at Monte Cimino, northern Lazio, Italy. Journal of Volcanology and Geothermal Research 158, 307–320.

Leocat, E., 2011. Histoire Eruptive des Volcans du Secteur Occidental des Iles Eoliennes (Sud de la Mer Tyrrhenienne, Italie) (Ph.D. thesis). University of Paris 11, Orsay (in French and English).

Losito, R., 1989. Stratigrafia, Caratteri Deposizionali e Aree Sorgente dei Tufi Bruni delle Isole Eolie (Ph.D. thesis). University of Bari, Italy (in Italian).

Lowe, D.R., 1982. Sediment gravity flows: II. Depositional models with special references to deposits of high-density turbidity currents. Journal of Sedimentary Petrology 52, 279–297.

Lube, G., Cronin, S.J., Platz, T., Freundt, A., Procter, J.N., Henderson, C., Sheridan, M.F., 2007. Flow and deposition of pyroclastic granular flows: a type example from the 1975 Ngauruhoe eruption, New Zealand. Journal of Volcanology and Geothermal Research 161, 165–186.

Lube, G., Breard, E.C.P., Jones, J., Fullard, L., Dufek, J., Cronin, S.J., Wang, T., 2019. Generation of air lubrication within pyroclastic density currents. Nature Geoscience 12, 381-386.

Lube, G., Breard, E.C.P., Esposti-Ongaro, T., Dufek, J., Brand, B., 2020. Multiphase flow behaviour and hazard prediction of pyroclastic density currents. Nature Reviews Earth & Environment 1, 348-365.

Lucchi, F., 2009. Late-Quaternary marine terrace deposits as tools for wide-scale correlation of unconformity-bounded units in the volcanic Aeolian archipelago (southern Italy). Sedimentary Geology 216, 158–178.

Lucchi, F., 2013. Stratigraphic methodology for the geological mapping of volcanic areas: insights from the Aeolian archipelago (southern Italy). Geological Society London Memoirs 37, 37–55.

Lucchi, F., Tranne, C.A. Calanchi, N., Pirazzoli, P.A., Romagnoli, C., Radtke, U., Reyss, J.L., Rossi, P.L., 2004. Stratigraphic constraints to date late-Quaternary ancient shorelines and to evaluate vertical movements at Lipari (Aeolian Islands). Quaternary International 115/116, 105–115.

1027 Lucchi, F., Tranne, C.A., De Astis, G., Keller, J., Losito, R., Morche, W., 2008. Stratigraphy and
1028 significance of Brown Tuffs on the Aeolian Islands (southern Italy). Journal of Volcanology
1029 and Geothermal Research 177, 49-70.
1030 Lucchi, F., Gertisser, R., Keller, J., Forni, F., De Astis, G., Tranne, C.A., 2013a. Eruptive history and
1031 magmatic evolution of the island of Salina (central Aeolian archipelago). Geological Society
1032 London Memoirs 37, 155-211.
1033 Lucchi, F., Keller, J., Tranne, C., 2013b. Regional stratigraphic correlations across the Aeolian
1034 archipelago (southern Italy). Geological Society London Memoirs 37, 55-81.
1035 Lucchi, F., Tranne, C.A., Peccerillo, A., Keller, J., Rossi, P.L., 2013c. Geological history of the
1036 Panarea volcanic group (eastern Aeolian archipelago). Geological Society London Memoirs 37,
1037 349-393.
1038 Lucchi, F., Peccerillo, A., Tranne, C.A., Rossi, P.L., Frezzotti, M.L., Donati, C., 2013d. Volcanism,
1039 calderas, and magmas of the Alicudi composite volcano (western Aeolian archipelago).
1040 Geological Society London Memoirs 37, 83–111.
1041 Lucchi, F., Santo, A.P., Tranne, C.A., Peccerillo, A., Keller, J., 2013e. Volcanism, magmatism,
1042 volcano-tectonics and sea-level fluctuations in the geological history of Filicudi (western
1043 Aeolian archipelago). Geological Society London Memoirs 37, 113-153.
1044 Mangeney, A., Roche, O., Hungr, O., Mangold, N., Faccanoni, G., Lucas, A., 2010. Erosion and
1045 mobility in granular collapse over sloping beds, Journal of Geophysical Research-Earth 115,
1046 F03040. https://doi.org/10.1029/2009JF001462.
1047 Manetti, P., Pasquaré, G., Tibaldi, A., Tsegaye, A., 1988. Geology of the island of Filicudi (Aeolian
1048 arc). Bollettino G.N.V. (Gruppo Nazionale di Vulcanologia, Italia) IV, 368-382.
1049 Manetti, P., Pasquaré, G., Tibaldi, A., Tsegaye, A., 1995. A new geo-vulcanological map of Filicudi
1050 island (Aeolian arc, Italy). Acta Vulcanologica 7, 1-5.

1051 Mathisen, M.E., Vondra, C.F., 1983. The fluvial and pyroclastic deposits of the Cagayan basin,
1052 Northern Luzon, Philippines—an example of non-marine volcaniclastic sedimentation in an
1053 interarc basin. Sedimentology 30, 369–392.
1054 Mele, D., Dioguardi, F., Dellino, P., Isaia, R., Sulpizio, R., Braia, G., 2015. Hazard of pyroclastic
1055 density currents at the Campi Flegrei Caldera (Southern Italy) as deduced fromthe combined
1056 use of facies architecture, physical modeling and statistics of the impact parameters. Journal of
1057 Volcanology and Geothermal Research 299, 35–53.
1058 Meschiari, S., Albert, P.G., Lucchi, F., Sulpizio, R., Smith, V.C., Kearne, R., Tranne, C.A., 2020.
1059 Frequent activity on Vulcano (Italy) spanning the last 80 ky: New insights from the chemo-
1060 stratigraphy of the Brown Tuffs. Journal of Volcanology and Geothermal Research 406.
1061 https://doi.org/10.1016/ j.jvolgeores.2020.107079.
1062 Miall, A.D., 1978. Lithofacies types and vertical profiles models in braided river deposits: a summary.
1063 In: Miall, A.D. (Ed.), Fluvial Sedimentology. Canadian Society of Petroleoum Geologists,
1064 Memoirs 5, 597–604.
1065 Miall, A.D., 1985. Architectural-element analyses: a new method of facies analyses applied to fluvial
1066 deposits. Earth-Science Reviews 22, 261–308.
1067 Mills, P.C., 1983. Genesis and diagnostic value of soft-sediment deformation structures: a review.
1068 Sedimentary Geology 35, 83–104.
1069 Morche, W., 1988. Tephrochronologie der Aolischen Inseln (Ph.D. thesis). Albert-Ludwigs-
1070 Universitat Freiburg, Germany (in German).
1071 Nichols, R., Sparks, R., and Wilson, C., 1994. Experimental studies of the fluidization of layered
1072 sediments and the formation of fluid escape structures. Sedimentology 41, 233–253.
1073 Odonne, F., Callot, P., Debroas, E.-J., Sempere, T., Hoareau, G., and Maillard, A., 2011. Soft-
1074 sediment deformation from submarine sliding: Favourable conditions and triggering
1075 mechanisms in examples from the Eocene Sobrarbe delta (Ainsa, Spanish Pyrenees) and the
1076 mid-Cretaceous Ayabacas Formation (Andes of Peru). Sedimentary Geology 235, 234–248.

1077 Owen, G., 1987. Deformation processes in unconsolidated sands. Geological Society London, Special
1078 Publications 29, 11–24.
1079 Peccerillo, A., De Astis, G., Faraone, D., Forni, F., Frezzotti, M.L., 2013. Compositional variations
1080 of magmas in the Aeolian arc: implications for petrogenesis and geodynamics. Geological
1081 Society London, Memoirs 37, 489–508.
1082 Pichler, H., 1980. The Island of Lipari. Rendiconti della Società Italiana di Mineralogia e Petrologia
1083 36, 415-440.
1084 Pollock, N.M., Brand, B.D., Rowley, P.J., Sarocchi, D., Sulpizio, R., 2019. Inferring pyroclastic
1085 density current flow conditions using syn-depositional sedimentary structures. Bulletin of
1086 Volcanology 81, 46. http://dx.doi.org/10.1007%2Fs00445-019-1303-z
1087 Kowalczuk, P.B., Drzymala, J., 2016. Physical meaning of the Sauter mean diameter of spherical
1088 particulate matter. Particulate Science and Technology 34, 645-647.
1089 Roche, O, 2015. Nature and velocity of pyroclastic density currents inferred from models of
1090 entrainment of substrate lithic clasts. Earth Planetary and Science Letters 418, 115-125.
1091 Roche, O., Montserrat, S., Niño, Y., Tamburrino, A., 2008. Experimental observations of water-like
1092 behaviour of initially fluidized, unsteady dense granular flows and their relevance for the
1093 propagation of pyroclastic flows. Journal of Geophysical Research 113, B12203.
1094 http://dx.doi.org/10.1029/2008JB 005664.
1095 Roche, O., Niño, Y., Mangeney, A., Brand, B.D., Pollock, N.M., Valentine, G.A., 2013. Dynamic
1096 pore-pressure variations induce substrate erosion by pyroclastic flows. Geology 41, 1107–1110.
1097 Roche, O., Buesch, D.C., Valentine, G.A., 2016. Slow-moving and far-travelled dense pyroclastic
1098 flows during the Peach Spring super-eruption. Nature Communications 7, 10890. doi:
1099 10.1038/ncomms10890
1100 Roche, O., Azzaoui, N., Guillin, A., 2021. Discharge rate of explosive volcanic eruption controls
1101 runout distance of pyroclastic density currents. Earth and Planetary Science Letters 568,
1102 117017. https://doi.org/10.1016/j.epsl.2021.117017

1103 Røe, S.-L., Hermansen, M., 2006. New aspects of deformed cross-strata in fluvial sandstones:
1104 examples from Neoproterozoic formations in northern Norway. Sedimentary Geology 186,
1105 283–293.
1106 Rohling, E.J., Foster, G.L., Grant, K.M., Marino, G., Roberts, A.P., Tamisiea, M.E., Williams, F.,
1107 2014. Sea-level and deep-sea-temperature variability over the past 5.3 million years. Nature
1108 508, 477–482.
1109 Rowley, P.J., Kokelaar, P., Menzies, M., Waltham, D., 2011. Shear derived mixing in dense granular
1110 flows. Journal of Sedimentary Research 81, 874–884.
1111 Sauter, J., 1926. Die Grössenbestimmung der in Gemischnebeln von Verbrennungskraftmaschinen
1112 vorhandenen Brennstoffteilchen. VDI-Verlag, Berlin, Forschungsarbeiten auf dem Gebiete des
1113 Ingenieurwesens, 279 pp (in German).
1114 Selker, J.S., 1993. Expressions for the formation of load casts in soft sediment. Journal of
1115 Sedimentary Research 63, 1149–1151.
1116 Smith, G.A., 1986. Coarse-grained nonmarine volcaniclastic sediment: terminology and depositional
1117 process. Geological Society of America Bulletin 97, 1–10.
1118 Smith, G.A., 1987. The influence of explosive volcanism on fluvial sedimentation: the Deschutes
1119 formation (Neogene) in central Oregon. Journal of Sedimentary Petrology 57, 613–629.
1120 Smith, G.M., Williams, R., Rowley, P.J., Parsons, P.D., 2018. Investigation of variable aeration of
1121 monodisperse mixtures: implications for pyroclastic density currents. Bulletin of Volcanology
1122 80, 67. https://doi.org/10.1007/s00445-018-1241-1
1123 Sohn, Y.K., Chough, S.K., 1989. Depositional processes of the Suwolbong Tuff Ring, Cheju Island
1124 (Korea). Sedimentology 36, 837–855.
1125 Sohn, Y.K., 1997. On traction carpet sedimentation. Journal of Sedimentary Research 67, 502–509.
1126
1127 Sulpizio, R., Dellino, P., 2008. Sedimentology, depositional mechanisms and pulsating behaviour of
1128 pyroclastic density currents. Developments in Volcanology 10, 57–96.

1129 Sulpizio, R., Mele, D., Dellino, P., La Volpe, L., 2007. Deposits and physical properties of pyroclastic
1130 density currents during complex Subplinian eruptions: the AD 472 (Pollena) eruption of
1131 Somma-Vesuvius, Italy. Sedimentology 54, 607–635.
1132 Sulpizio, R., De Rosa, R., Donato, P., 2008a. The influence of variable topography on the depositional
1133 behaviour of pyroclastic density currents: the examples of the Upper Pollara eruption (The
1134 island of Salina, southern Italy). Journal of Volcanology and Geothermal Research 175, 367–
1135 385.
1136 Sulpizio, R., Bonasia, R., Dellino, P., Di Vito, M.A., La Volpe, L., Mele, D., Zanchetta, G., Sadori,
1137 L., 2008b. Discriminating the-long distance dispersal of fine ash from sustained columns or
1138 near ground ash clouds: the example of the Pomici di Avellino eruption (Somma-Vesuvius,
1139 Italy). Journal of Volcanology and Geothermal Research, 177, 263-276. doi:
1140 10.1016/j.jvolgeores.2007.11.012
1141 Sulpizio, R., Bonasia, R., Dellino, P., Mele, D., Di Vito, M.A., La Volpe, L., 2010. The Pomici di
1142 Avellino eruption of Somma-Vesuvius (3.9 ka BP). Part II: Sedimentology and physical
1143 volcanology of pyroclastic density current deposits. Bulletin of Volcanology 72, 559–577.
1144 Sulpizio, R., Alçiçek, M.C., Zanchetta, G., Solari, L., 2013. Recognition of the Minoan tephra in
1145 Acigöl Basin, Western Turkey: implications for inter archive correlations and fine ash dispe.
1146 Journal of Quaternary Science, 28, 329-336.
1147 Sulpizio, R., Dellino, P., Doronzo, D.M., Sarocchi D., 2014. Pyroclastic density currents: state of the
1148 art and perspectives. Journal of Volcanology and Geothermal Research 283, 36–65.
1149 Sulpizio, R., Castioni, D., Rodriguez-Sedano, L.A., Sarocchi, D., Lucchi, F., 2016. The influence of
1150 slope-angle ratio on the dynamics of granular flows: insights from laboratory experiments.
1151 Bulletin of Volcanology 78, 77. https://doi.org/10.1007/s00445-016-1069-5
1152 Tomlinson, E.L., Albert, P.G., Wulf, S., Brown, R., Smith, V.C., Keller, J., Orsi, G., Bourne, A.J.,
1153 Menzies, M.A., 2014. Age and geochemistry of tephra layers from Ischia, Italy: constraints

from proximal-distal correlations with Lago Grande di Monticchio. Journal of Volcanology and Geothermal Research 287, 22-39.

Valentine, G.A., 1987. Stratified flow in pyroclastic surges. Bulletin of Volcanology 49, 616–630.

Valentine, G.A., Buesch, D.C., Fisher, R.V., 1989. Basal layered deposits of the Peach Springs Tuff, northwestern Arizona, USA. Bulletin of Volcanology 51, 395–414.

Ventura, G., 2013. Kinematics of the Aeolian volcanism (Southern Tyrrhenian Sea) from geophysical and geological data. Geological Society London, Memoirs 37, 3–11.

Waelbroeck, C., Labeyrie, L., Michel, E., Duplessy, J.C., McManus, J.F., Lambeck, K., Balbon, E., Labracherie, M., 2002. Sea-level and deep water temperature changes derived from foraminifera isotopic records. Quaternary Science Reviews 21, 295–305.

Waresback, D.B., Turbeville, B.N., 1990. Evolution of a Plio-Pleistocene volcanogenic alluvial fan: the Puye formation, Jemez Mountains, New Mexico. Geological Society America Bulletin 102, 298–314.

TABLES

Tab. 1. Selected outcrops, stratigraphy and measurements of the sin-depositional sedimentary structures. The distance from the source area is arbitrarily measured relative to the centre of the La Fossa Caldera. The sample names refer to the BT depositional units selected for chemical analyses. Labels for the sedimentary structures: MB=mixing band; US=undulated structure; FS=recumbent flame structure; RS=rip-up structure. In the column of sedimentary structures, the symbol / indicates that there is no direct evidence in the field of mixed lithofacies, but the process of clast-embedding is outlined by means of geochemical analyses.

Tab. 2. Lithofacies codes, description and interpretation of the lithofacies recognised in the BT investigated in the present work. The first letters of the lithofacies code indicate the general

1180 appearance of the deposit (m = massive, ps = planar stratified, xs = cross-stratified, is = intermittently
1181 stratified, etc.) and the capital letters indicate the grain size (A = ash, L = lapilli).
1182
1183 **Tab. 3.** Grain size statistical parameters of Folk and Ward (1957) for the different sub-populations
1184 recognised in the samples from the base of some BT depositional units: BT=Brown Tuffs; mg=Monte
1185 Guardia unit; lpt=Lower Pollara Tuffs; fa=Falcone unit. The parameters by Folk and Ward (1957)
1186 were calculated by means of the GRADISTAT program (Blott and Pye, 2001). The Sauter mean
1187 diameter (Sauter 1926) of the different BT sub-populations is estimated using the method of Breard
1188 et al. (2019).
1189
1190 **FIGURES**
1191
1192 **Fig. 1.** Sketch maps of the islands of Vulcano and Lipari (A) showing the areal distribution of the BT
1193 deposits and the location of outcrops where the sedimentary structures object of the present study
1194 have been observed (L1-13, V1-6). The inset (B) shows the location of the Aeolian Islands and
1195 seamounts in the southern Tyrrhenian sea (depth contour lines in metres below sea level). Coordinates
1196 conform to the Gauss-Boaga System (IGM). In (C) there is a sketch chronostratigraphic framework
1197 showing the development of Aeolian subaerial volcanism and the time-stratigraphic interval of BT
1198 deposition. Labels for the main tephra layers are: pt = Petrazza Tuffs; gpt = Grey Porri Tuffs; it =
1199 Ischia Tephra; lpt = Lower Pollara Tuffs; gu = Monte Guardia pumice; vg = Vallone del Gabellotto
1200 pumice; pn = Punte Nere tuffs. References: Alicudi = Lucchi et al. (2013c); Filicudi = Lucchi et al.
1201 (2013d); Salina = Lucchi et al. (2013a); Lipari = Forni et al. (2013); Panarea = Lucchi et al. (2013b);
1202 Vulcano = De Astis et al. (2013); Stromboli = Francalanci et al. (2013).
1203
1204 **Fig. 2.** Generalized stratigraphic succession of the BT derived from correlations between the islands
1205 of Lipari and Vulcano. The BT succession is subdivided into (at least) 16 depositional units (BT1-

16) superposed to the LBT, IBT, IBT-upper and UBT macro-units by means of interlayered volcanic units and tephra layers, erosive surfaces and reworked horizons (see also Meschiari et al., 2020). The individual depositional units of the UBT on Vulcano have a different name because they cannot be directly correlated with those on Lipari. References for the stratigraphy of the two islands are: Forni et al., 2013 (Lipari); De Astis et al., 2013 (Vulcano). The stratigraphic units interlayered within the BT that are characterised by the sedimentary structures object of this work are described in Table 1.

Fig. 3. Outcrop photographs of the BT and their distinctive lithofacies. A) Massive deposits (lithofacies mA) of the BT on Lipari (outcrop L5). The BT in this outcrop correspond to the IBT-upper and UBT macro-units developed above the Monte Guardia marker bed. B) UBT deposits on Vulcano (outcrop V1) characterised by planar to cross-stratified lithofacies (psA-xsA). C) Alternating massive (mA) and intermittently stratified (isA) lithofacies of the UBT on Vulcano (outcrop V3). D) Detailed view of the deposits of Figure 3C. E) Detail of the ruptured laminae of the intermittently stratified deposits of UBT. The arrows indicate distinctive upward bending of the laminae in the rupture points. F) Intermittently stratified ash (isA) deposits of the UBT on Vulcano (outcrop V2). G) Close view of the deposits of Figure 3G showing ruptured laminae with typical upward deformation and columns of coarse ash (arrow) and inflated deformation of the laminae before the rupture (*). H) Close view of the deposits of Figure 3G showing ruptured laminae with typical upward deformation (arrow). I) Massive deposits of the UBT on Vulcano near to Grotta dei Pisani that contain fragments of laminae (arrows) representing relicts of the stratified lithofacies.

Fig. 4. Field evidence of the mixing bands recognised at base of different BT depositional units on Lipari and Vulcano, shown in stratigraphic order (starting from the oldest) according to Fig. 2. A) Vallone dei Lacci, Lipari (outcrop L8): mixing band (*) between the BT4 depositional unit and the Grey Porri Tuffs (gpt). B) Valle Muria, Lipari (outcrop L2): mixing band (*) between the BT8 depositional unit and the Punta del Perciato pumice (pe). C) Mixing band (*) between the BT9

depositional unit and the Falcone pumice (pe) at Valle Muria, Lipari (outcrop L2). D) Detail of the mixing band in Figure 4C. E) Spiaggia Valle Muria, Lipari (outcrop L1): mixing band (*) between the BT9 depositional unit and the Falcone pumice (pe). F) Valle Muria, Lipari (outcrop L2): scattered pumice lapilli of the Falcone unit (fa) embedded within the overlying BT9 depositional unit. G) Gelso, Vulcano (outcrop V5): mixing band (*) between the BT12 depositional unit and the Monte Guardia tephra layer (gu). H) Passo del Piano, Vulcano (outcrop V1): mixing band (*) between the BT16(V) depositional unit and the Vallone del Gabellotto pumice (vg).

Fig. 5. Field evidence of shear structures on Lipari. A) Tunnel Canneto, Lipari (outcrop L5): undulated structure (lithofacies ucAL) along the contact between the BT12 depositional unit and the underlying Monte Guardia pumice succession. B) Crest of the undulated structure of Figure 5A. In the inset it is shown a zoom on the crest of the undulated structure made up of mixed material between the BT12 and the underlying incoherent pyroclastic deposit. C) Spiaggia Valle Muria, Lipari (outcrop L1): panoramic view of the undulated structure (lithofacies ucAL) along the contact between the BT9 depositional unit and the underlying Falcone pumice succession. D) Trail of pumice and lithic lapilli of the Falcone pumice succession embedded within the overlying BT9 depositional unit (see C for location), representing the tail of a recumbent flame structure (lithofacies rfAL). E) Deformed bed of mixed material between the BT9 depositional unit and pumice lapilli from the underlying Falcone succession, representing the trunk of a not fully developed recumbent flame structure (lithofacies rfAL). F) Detail of the undulated contact in Figure 5C showing a hook-like structure of rip-up lapilli from the underlying Falcone unit (lithofacies ruAL).

Fig. 6. Grain-size and components frequency histograms of weight % at half-phi intervals and pie charts of the components of representative samples of the mixing bands at the base of distinct BT depositional units in outcrops L2, L5, L10 and L12 on Lipari (see Fig. 1A for location).

Representative photographs of the outcrops are also shown. The outcrops are displayed relative to an increasing distance from the inferred source area of La Fossa Caldera on Vulcano from base to top.

Fig. 7. TAS (A) and K_2O/SiO_2 (B) classification diagrams of the BT glasses compared to the volcanic glasses of explosive eruption deposits produced on Vulcano, Lipari and Salina during the last 50 ky. Data for the BT glasses are from Meschiari et al. (2020), whislt the data for Vulcano, Lipari and Salina are from Albert et al. (2017). Error bars represent 2*standard deviations of replicated analyses of the StHs6/80-G secondary standard glass run alongside the BT samples. The secondary components recognised in distinct BT depositional units referred to the LBT, IBT, IBT-upper and UBT macro-units are compared to the compositions of the underlying proximal pyroclastic units in distinct major element glass geochemical variation diagrams (A-N). The stratigraphic succession of BT depositional units (BT3, BT4, BT8, BT9, BT10, BT12, BT14-V, BT16-V) refers to Fig. 2. Data for the BT glasses are from Meschiari et al. (2020). References for the pyroclastic units used for comparison are: Grey Porri Tuffs (w.r.) = Sulpizio et al. (2016); Grey Porri Tuffs, Salina, proximal = Albert et al. (2017); Grey Porri Tuffs, Lipari medial, Vulcano medial-distal and Panarea, distal = Sulpizio et al., 2016; Meschiari et al. (2020); Lip1 = Meschiari et al. (2020); Falcone = Albert et al. (2017); Punta del Perciato = Albert et al. (2017); Monte Guardia field = Albert et al. (2017) and Meschiari et al. (2020); Monte Guardia (1) = Albert et al. (2017); Monte Guardia (2) = Meschiari et al. (2020); Cugni di Molinello = Meschiari et al. (2020); Vallone del Gabellotto (1) = Albert et al. (2017); Vallone del Gabellotto (2) = Meschiari et al. (2020).

Fig. 8. Sketch of the transport and depositional behaviour of the PDCs during the UBT eruptions on Vulcano island when interacting with the La Fossa Caldera wall (arrows indicate the flow direction). In the inbox, a model explaining the formation of lithofacies altpsmA (alternance of planar stratified and massive ash) as continuous aggradation of deposits from different PDC pulses (a, b, c, d) in the area of il Piano to the south of the source area, and the lithofacies isA

(intermittently stratified ash) as disruption of the deposits due to fluid escape (d, e, f). Not to scale.

Fig. 9. Sketch of the formation of syn-depositional sedimentary structures (mixing bands, undulated structures and recumbent flame structures) at the base of the BT deposits as the result of lateral transport and high shear stress exerted by the PDCs of the BT on the loose underlying pyroclastic (pumice) material along downslope and upslope paths on the island of Lipari, to the north of the La Fossa Caldera source area. Arrows indicate the flow direction. Not to scale.

Fig. 10. Sketch of the transport and depositional behaviour of the BT PDCs laterally spreading from the La Fossa caldera source on Vulcano towards the island of Lipari, crossing the narrow sea arm of the Bocche di Vulcano and interacting with the irregular paleo-topography of Lipari (see explanation in the text).

Fig. 11. Diagrams showing variations of minimum basal shear velocity (u_*) vs. relative flow concentration between PDCs and an underlying bed ($\boldsymbol{x} = \rho_{PDC}/\rho_{bed}$) for different wavelength numbers ($\lambda/2\pi$) of basal instabilities. Dashed lines indicate the minimum basal shear velocity for the observed wavelength of undulated structures of 40 cm ($\lambda/2\pi$=0.16) and 450 cm ($\lambda/2\pi$=0.72 as example of bed instabilities in the case study of the BT eruptions.

SUPPLEMENTARY MATERIAL

Supplementary File 1 - Main characteristics of tephra units used for the subdivisions of the BT succession and showing evidence of syn-depositional clast incorporation within distinct BT depositional units (listed in stratigraphic order starting from the older one). Chemical composition of juvenile glass fragments (w.r=whole rock) and mineralogy are reported by referring to: (1) present work; (2) Meschiari et al. (2020); (3) Albert et al (2017); (4) Sulpizio et al. (2016); (5) Tomlinson et

al. (2014); (6) De Astis et al (2013); (7) Gioncada et al. (2005); (8) De Rosa et al. (2003); (9) Calanchi et al. (1993). Labels for compositions: CA=calcalkaline, HKCA=high-k calcalkaline, SHO=shoshonite series; Bas-And=basaltic andesite, And=andesite, Dac=dacite, Rhy=rhyolite, Sho=shoshonite. Labels for phenocrysts: pl=plagioclase, kf=K-feldspar; cpx=clinopyroxene; opx=orthopyroxene, bt=biotite; ol=olivine; amp=amphibole; ox=oxides; ap=apatite; zr=zircon; ti=titanite; acm=acmite). Proximal stratigraphic units refer to: (1) Lucchi et al. (2008); (2) Forni et al. (2013); (3) Lucchi et al. (2013a); (4) De Astis et al. (2013). Age references: (1) Morche (1988); (2) Soligo et al. (2000); (3) Siani et al. (2004); (4) Leocat (2011); (5) Lucchi et al. (2013a; 2013b); (6) Sulpizio et al. (2016); (7) Giaccio et al. (2017); (8) Meschiari et al. (2020).

Supplementary File 2 - Representative major and minor element compositions of samples relative to the mixing bands recognised in this study at the base of different Brown Tuffs (BT) units, according to LBT, IBT, IBT-upper and UBT macro-units. Totals are pre-normalised analytical totals. For each of the samples, we include representative analyses for the main BT juvenile component and the secondary components (sec. comp.) relative to the process of clast embedding from the underlying pyroclastic units. Representative analyses for the proximal pyroclastic units used for the correlation of the secondary components are reported for comparison (in grey): gpt=Grey Porri Tuffs, Salina; pe=Punta del Perciato, Lipari; fa=Falcone, Lipari; Lip1 tephra layer, Lipari; mg=Monte Guardia, Lipari; cm=Cugni di Molinello, Vulcano; vg=Vallone del Gabellotto, Lipari. Compositions of the proximal pyroclastic units and the BT conform to Meschiari et al. (2020), except for "pe", "fa" and "mg" which are from Albert et al. (2017).

Highlights

- Sedimentological analysis of widespread ash-rich pyroclastic deposits
- Deposits from ground-hugging pulsating pyroclastic density currents (PDCs)
- Post-depositional disruption due to fluid escape and dissipation of pore pressure
- Erosion and clast embedding by PDCs at several kms away from the source area
- Shear-related granular instability structures at the base of PDC deposits

Figure 1

Click here to access/download;Figure;Fig. 1_lucchi.jpg

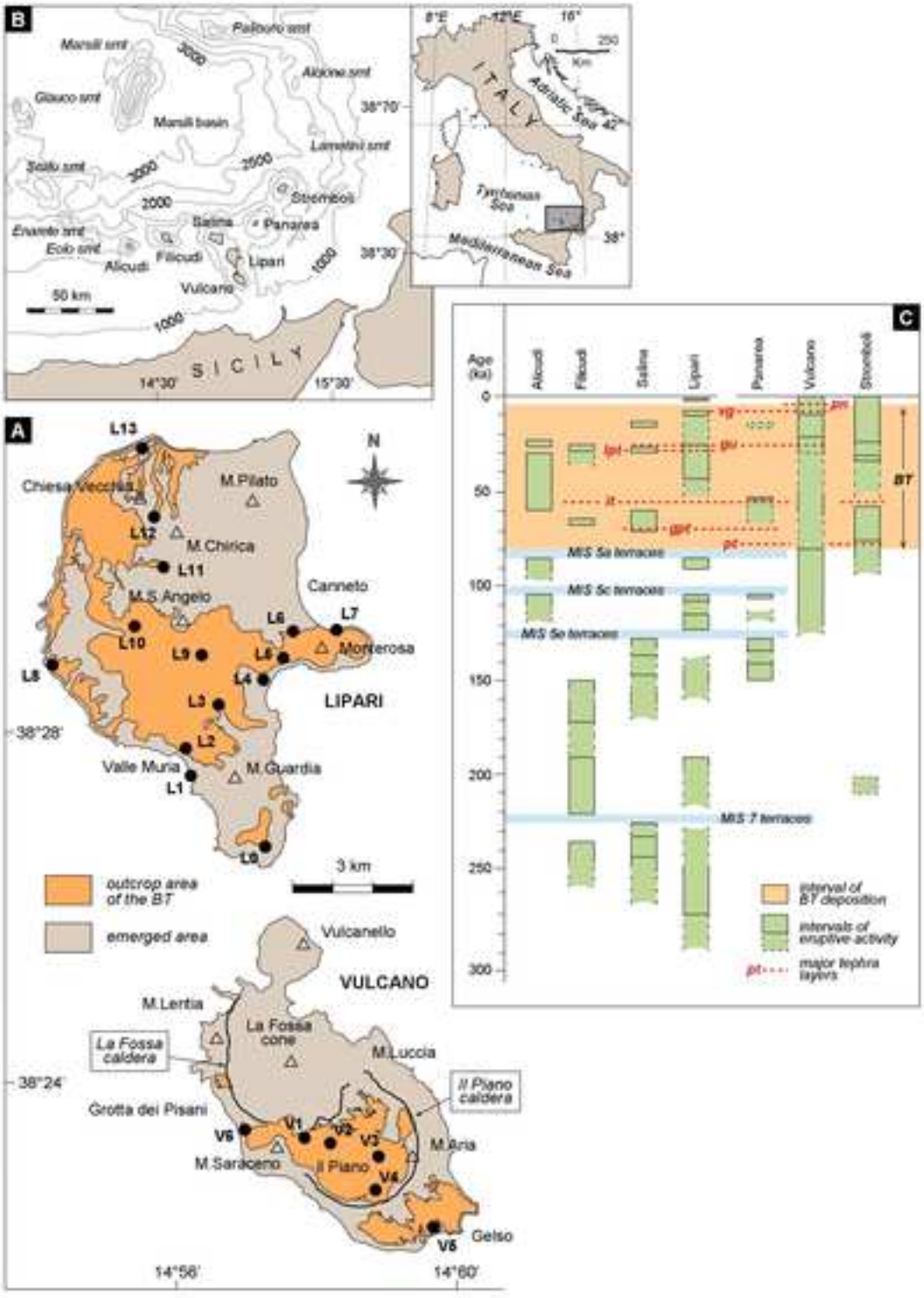

Fig. 1

Figure 2

Click here to access/download;Figure;fig. 2_lucchi.jpg

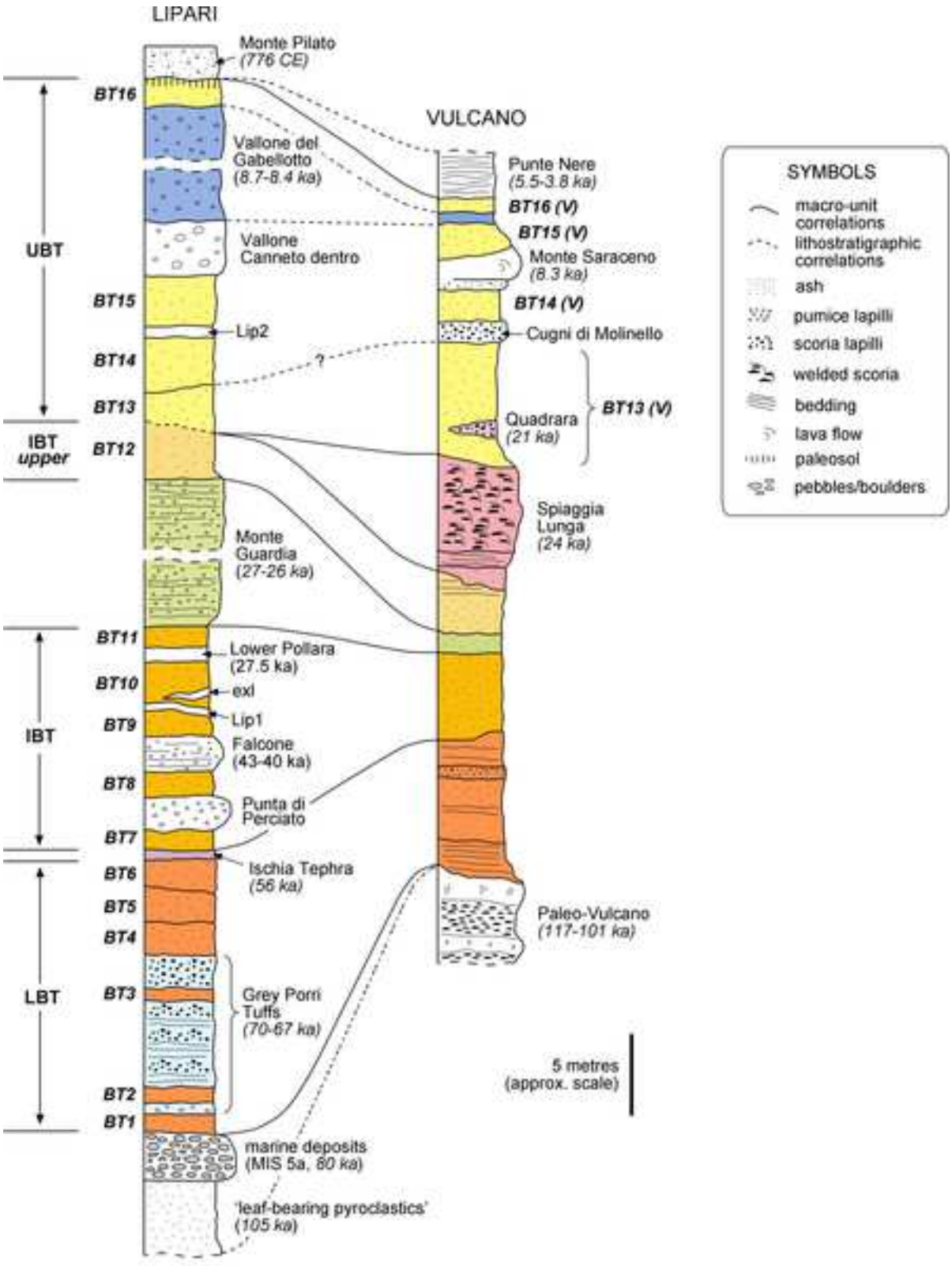

Fig. 2

Click here to access/download;Figure;fig. 3_lucchi.jpg

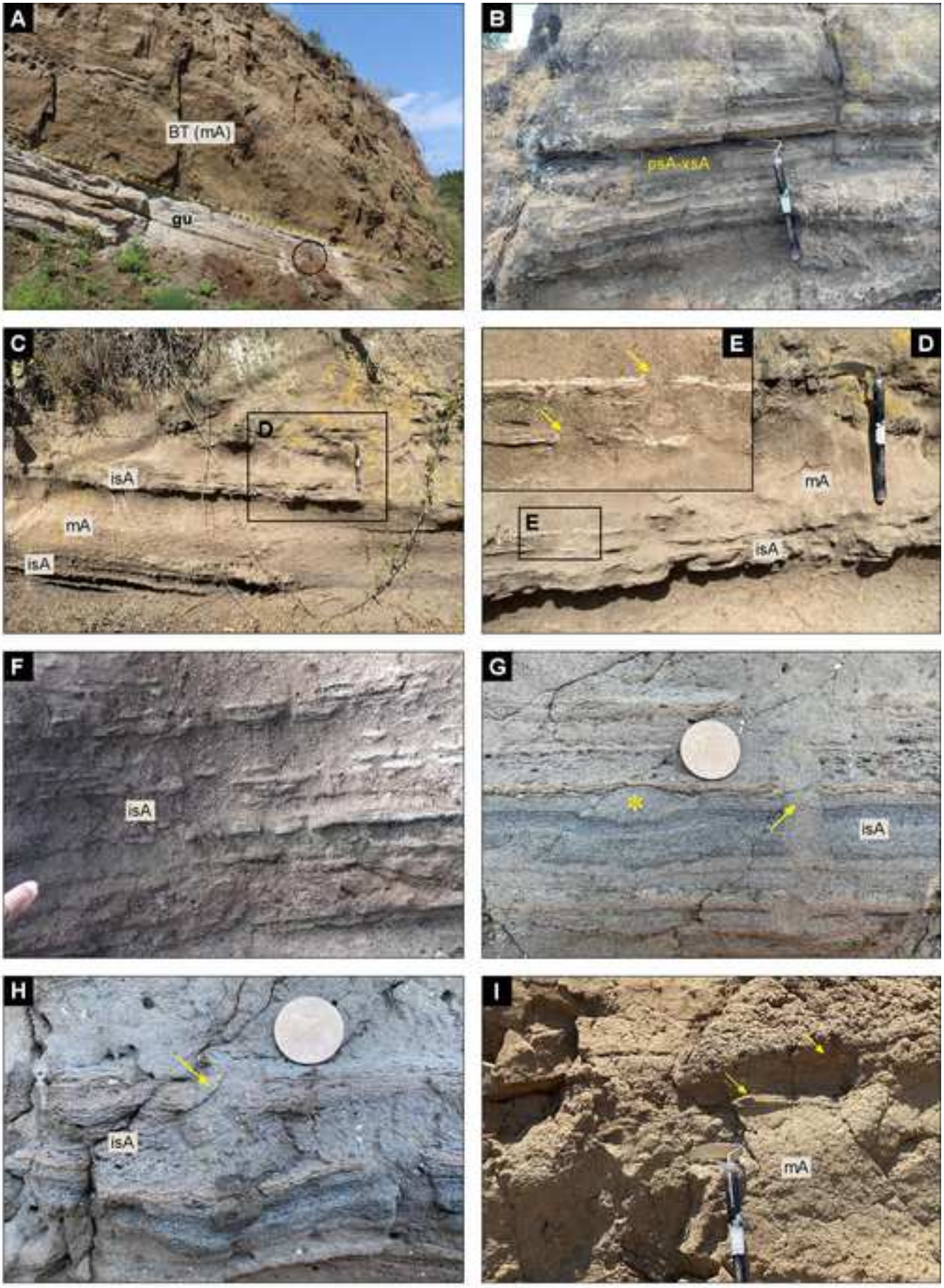

Fig. 3

Click here to access/download;Figure;fig. 4_lucchi.jpg

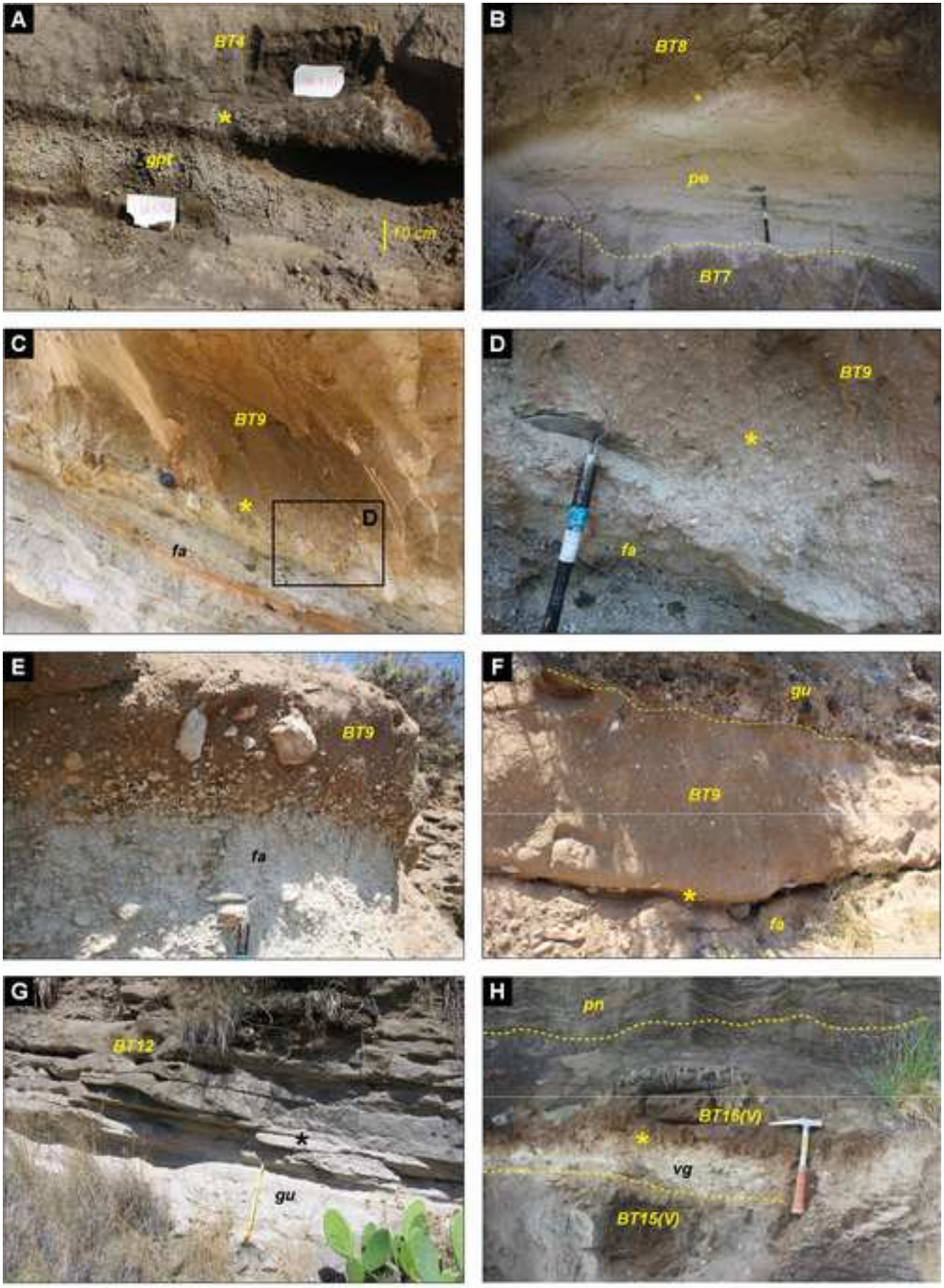

Fig. 4

Click here to access/download;Figure;fig. 5_lucchi.jpg

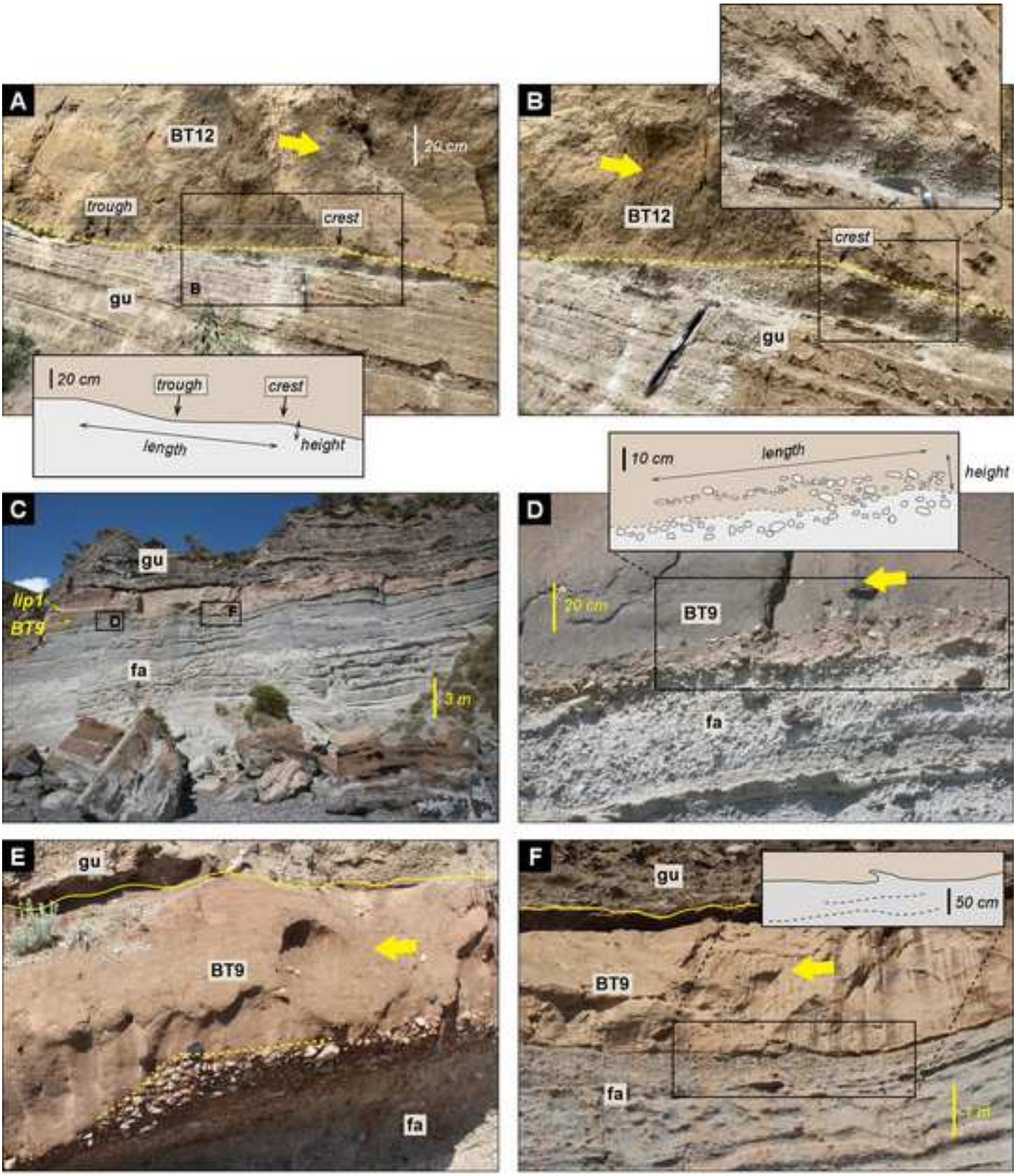

Fig. 5

Click here to access/download;Figure;fig. 6_lucchi.jpg

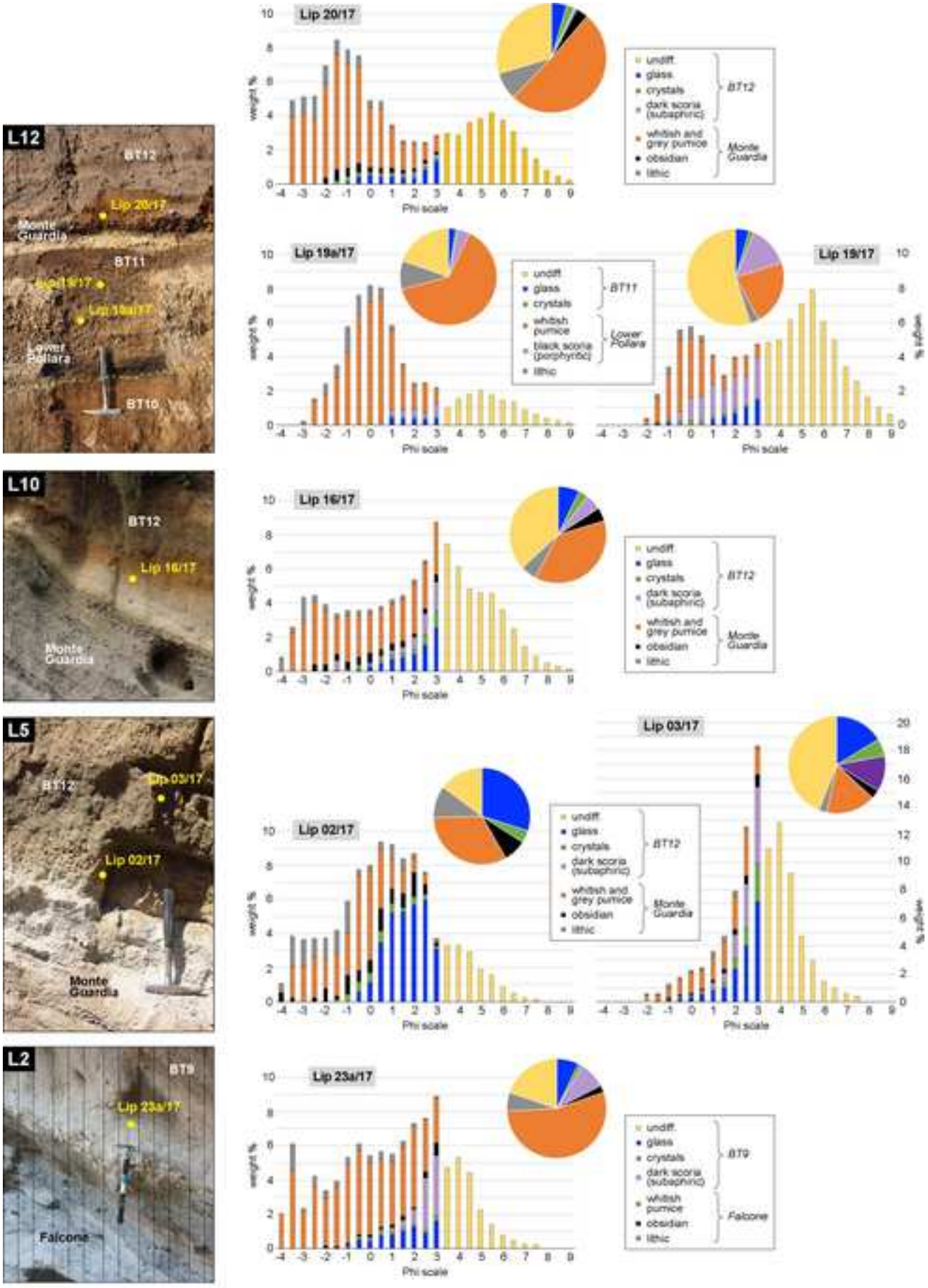

Fig. 6

Figure 7

Click here to access/download;Figure;fig. 7_lucchi.jpg

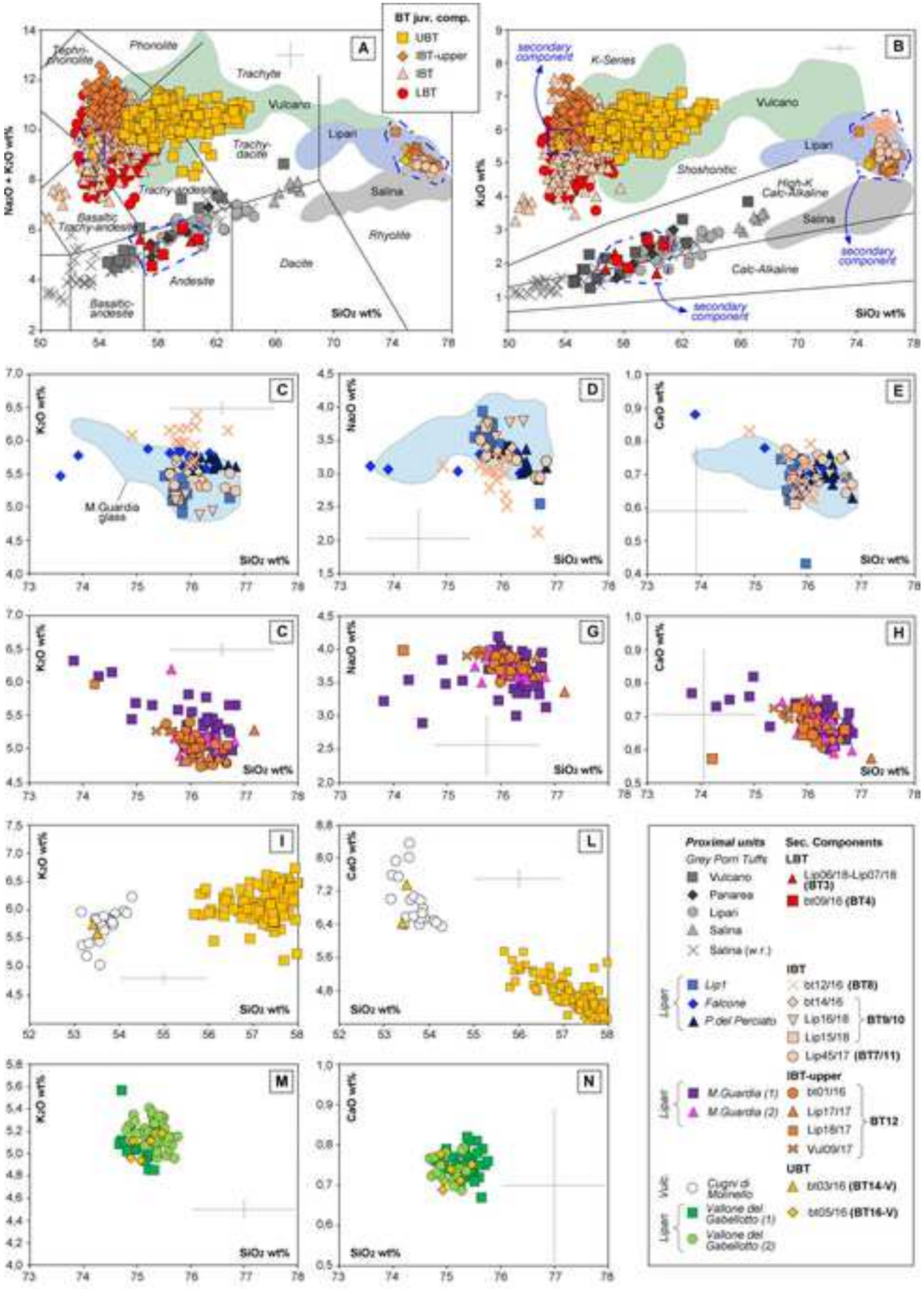

Fig. 7

Click here to access/download;Figure;fig. 8_lucchi.jpg

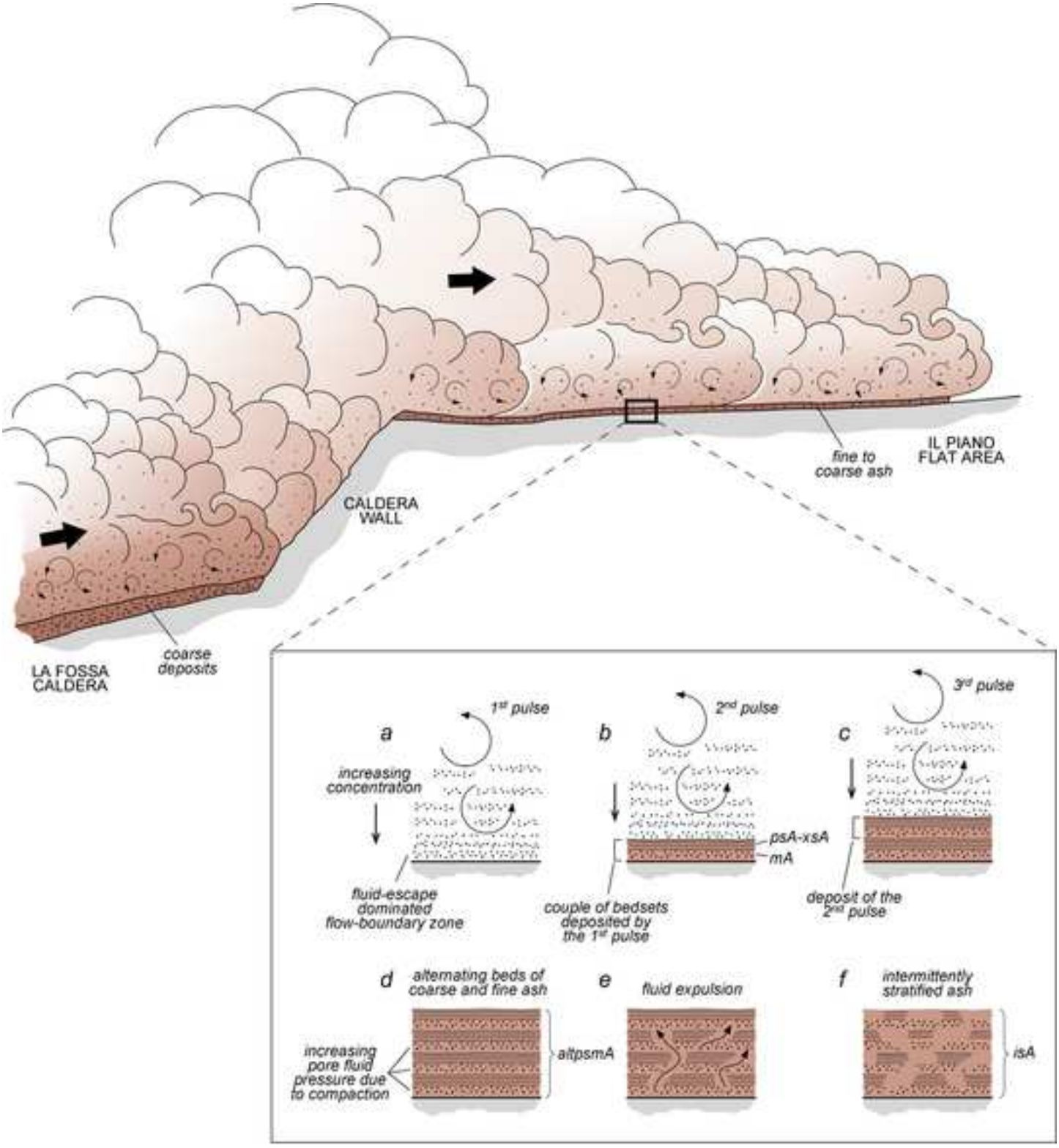

Fig. 8

Click here to access/download;Figure;fig. 9_lucchi.jpg

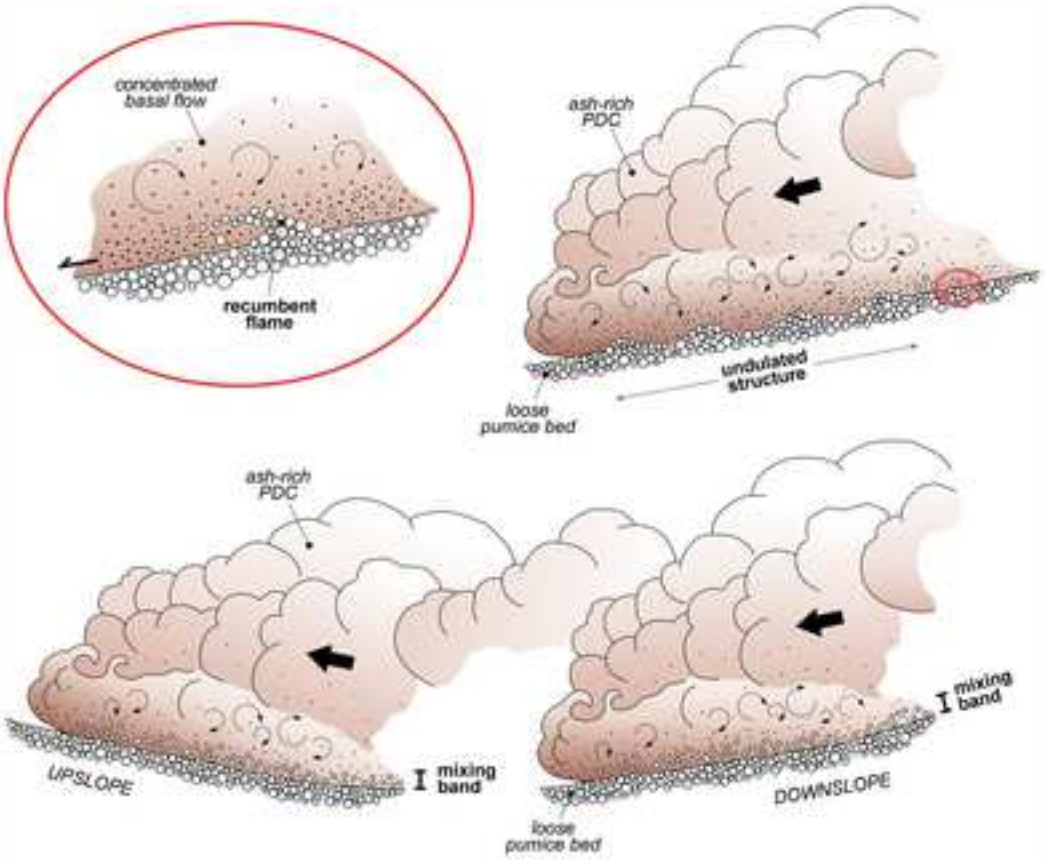

Fig. 9

Click here to access/download;Figure;fig. 10_lucchi.jpg

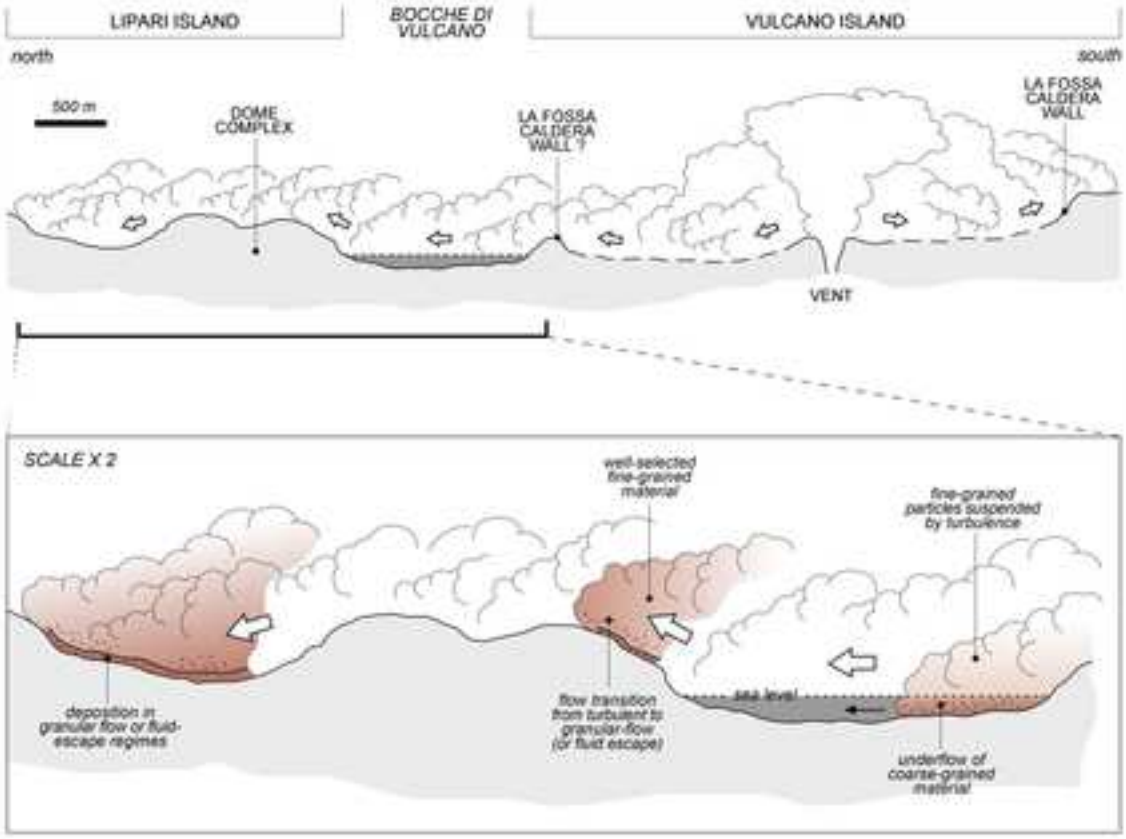

Fig. 10

Click here to access/download;Figure;Fig. 11_lucchi.tif

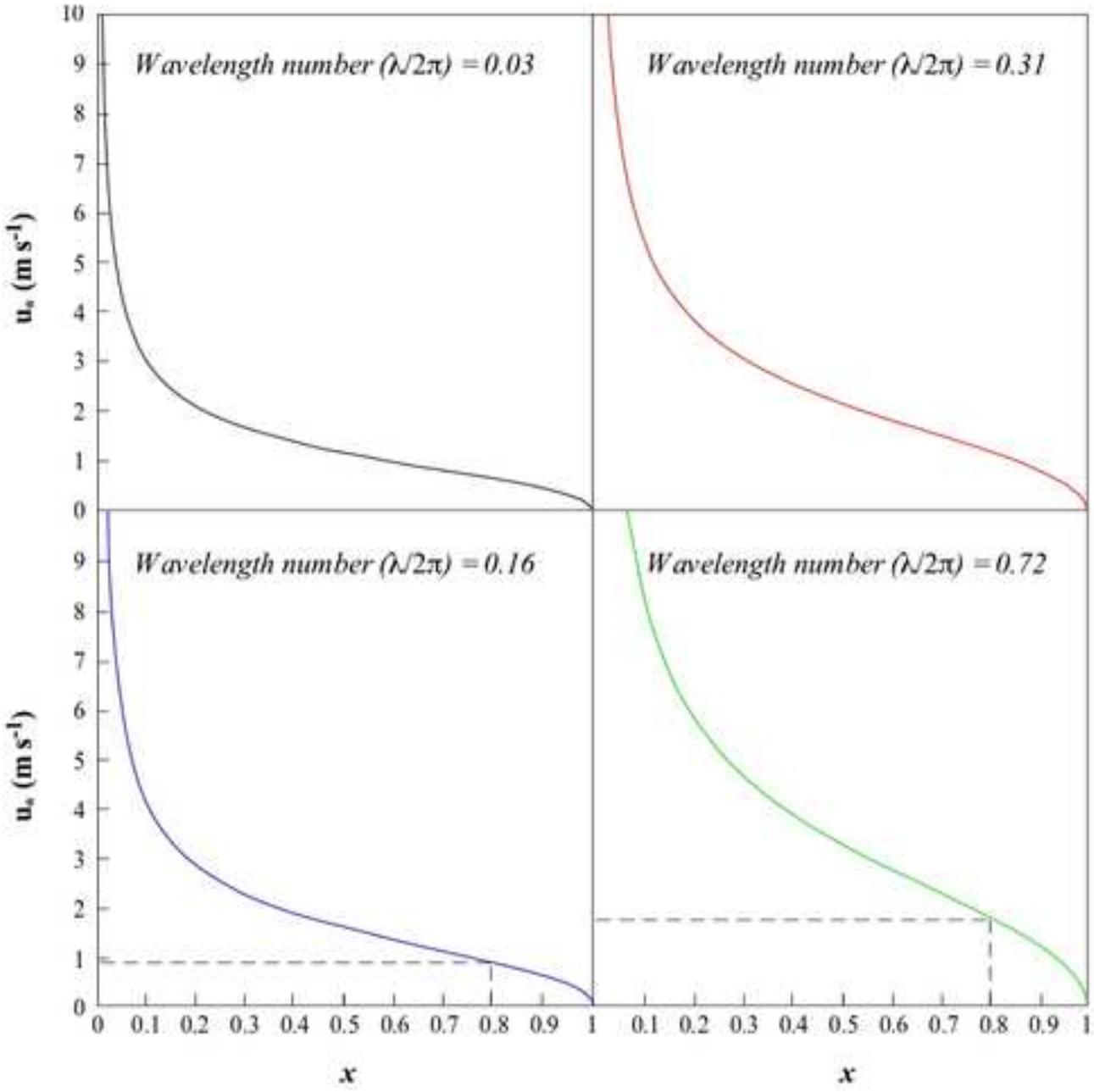

Fig. 11

Click here to access/download;Table;Table 1_lucchi.pdf

Table 1 - Selected outcrops, stratigraphy and measurements of the syn-depositional sedimentary structures. The distance from the source area is arbitrarily measured relative to the centre of the La Fossa Caldera. The sample names refer to the BT depositional units selected for chemical analyses. Labels for the sedimentary structures: MB=mixing band; US=undulated structure; FS=recumbent flame structure; RS=rip-up structure. In the column of sedimentary structures the symbol / indicates that there is no direct evidence in the field of mixed lithofacies but the process of clast-embedding is outlined by means of geochemical analyses.

Island	Outcrop	Location	Distance (km)	Sedimentary structure	BT dep. unit	Sample name	underlying unit	Thickness - MB (cm)	Length (cm)	Height (cm)
Lipari	L0	Punta della Crapazza	5,5	/	BT10	Lip15/18, Lip16/18, Lip17/18	Lip1*	/		
	L1	Spiaggia Valle Muria	7,7	MB, US, FS, RS	BT9		Falcone	≈30 (max)	≈450 (US)	≈20 (US)
									≈60 (FS)	≈20 (FS)
				MB	BT10		Lip1	≈5		
	L2	Valle Muria	8.5	MB	BT11		Lower Pollara	10		
				/	BT10	bt14/16	Lip1	/		
				MB	BT9		Falcone	25-30		
				MB	BT8	bt12/16	P. di Perciato	≈10		
	L3	Chiesa dell'Annunciazion	9.5	MB	BT12		Monte Guardia	≈25		
	L4	Portinente	10	MB	BT12	bt01/16	Monte Guardia	n.v.		
	L5	Tunnel Canneto	10.5	MB, US	BT12		Monte Guardia	≈15	≈250	≈20
	L6	Vallone Canneto dentro	11	MB	BT11		Lower Pollara Tuffs	≈5		
				MB	BT9		Falcone	≈10		
				MB	BT7		Ischia Tephra	≈5		
				MB	BT3-BT4	Lip06/18, Lip07/18	Grey Porri Tuffs	≈5		
	L7	Monterosa	11	/	BT9-10-11	Lip45/17	Lip1, Falcone or P. del Perciato	/		
				MB	BT7		Ischia Tephra	≈3		
	L8	Vallone dei Lacci	12	MB	BT4	bt09/16	Grey Porri Tuffs	≈5		
	L9	Santa Margherita	11	MB	BT11		Lower Pollara Tuffs	≈10		
	L10	Madoro	12	MB	BT12	Lip17/17, Lip18/17	Monte Guardia	≈25		
				MB	BT11		Lower Pollara Tuffs	≈10		
				MB	BT9		Falcone	≈5		
	L11	Vallone Fiume Bianco	13.5	MB	BT16		Vallone del Gabellotto	≈15		
	L12	Chiesa Vecchia	14.5	MB	BT12		Monte Guardia	≈5		
				MB	BT11		Lower Pollara Tuffs	≈5		
	L13	Acquacalda	16.5	MB	BT16		Vallone del Gabellotto	≈20		
					BT12		Monte Guardia	≈10		
Vulcano	V1	Passo del Piano	2	MB	BT16 (V)	bt05/06	Vallone del Gabellotto	≈10		
	V2	Il Piano	2.5	MB	BT14 (V)		Cugni di Molinello	≈10		
	V3	Il Piano	3	MB	BT14 (V)		Cugni di Molinello	≈10		
	V4	Serra dei Pisani	4	MB	BT14 (V)	bt03/16	Cugni di Molinello	≈15		
	V5	Gelso	5.7	MB	BT12	Vul09/17	Monte Guardia	≈20		
	V6	Grotta dei Pisani	2	/	BT13(V)		Spiaggia Lunga	/		

Table 2 - Lithofacies codes, description and interpretation of the lithofacies recognized in the BT investigated in the present work. The first letters of the lithofacies code indicate the general appearance of the deposit (m = massive, ps = planar stratified, xs = cross-stratified, is = intermittently stratified, etc.) and the capital letters indicate the grain size (A = ash, L = lapilli).

Lithofacies code	Description	Interpretation	Reference
mA	Massive, fine to coarse ash, sometimes with scattered pumice and lapilli. Abundant ash aggregates. Geochemically homogeneous. Moderate to poor sorting.	Gentle settling from a slow-moving, ground-hugging ash cloud. The homogeneous massive appearance suggests deposition from a fine-grained, concentrated flow-boundary zone dominated by fluid escape or granular flow regime. Ash aggregates indicate the presence of steam in the ash cloud or fine ash aggregation driven by electrostatic force during gentle settling of ash from the phoenix cloud of the PDCs.	Figs. 3A, C-D, I
xsA	Cross-stratified ash, sometimes with laminae. Dune bedded, medium to coarse ash. Moderate to good sorting	Dune-bedding and internal cross stratification indicate grain by grain deposition from a diluted, turbulent current in which suspension and traction are the main transport mechanisms.	Fig. 3B
psA	Planar stratified ash, sometimes with laminae. Moderate to good sorting	Planar stratification indicate grain by grain deposition from a diluted, turbulent current in which suspension and traction are the main transport mechanisms	Fig. 3B
altpsmA	Alternating planar stratified and massive ash. Planar stratified ash sometimes contains laminae. Moderate to good sorting.	The alternating beds of planar stratified and massive ash testifies for stepwise aggradation of discrete pulses developed within each depositional unit. The massive beds indicate that the flow-boundary zone of each pulse was dominated by granular- or fluid-escape dominated depositional regime. Planar stratified ash beds testify for sedimentation from the waning stage of each pulse, mainly in the traction regime.	
isA	Intermittently stratified ash. Alternation of mm to cm thick massive and stratified beds. The stratified beds are disrupted with distinctive upward deformation and vertical columns of coarse ash at the disruption points. Moderate to good sorting	Massive beds indicate deposition from a fluid-escape dominated flow boundary zone, whilst the stratified beds indicate deposition from a dilute, turbulent current in which suspension and traction are the main transport mechanisms. The disruption of stratified beds is driven by fluid escape structures related to post depositional dissipation of pore pressure from the underlying massive beds.	Figs. 3C-H
Shear structures			
mixAL	Mixed ash and lapilli from different units. The ash component is generally homogeneous and forms the matrix of the deposit. The lapilli (and ash) fraction is made by white pumice and dark scoriae eroded from the loose underlying units. Distribution of pumice and scoria may be homogeneous or their abundance decreases regularly upwards within the overlying ash. Massive and generally poorly sorted, with occasional reverse grading of entrained coarse	Mixing of material from different units indicate erosion and incorporation of loose material from the underlying beds into the moving ash flows. The general poor sorting and massive appearance are suggestive of sedimentation from a current in which the rate of supply (Rs) is higher than the rate of deposition (Rd). This induces the rapid development of a highly concentrated zone above the flow boundary, dominated by fluid escape or granular flow regimes. The moving flow exerted shear stress over the loose substratum, causing entrapment of clasts into the flow body. The occasional reverse grading of entrained coarse clasts reveals dispersive pressure	Figs. 4A-H

	clasts.	processes induced by grain-grain collision in a high-concentration zone at the base of the current.	
ucAL	Undulated contact between ash and underlying lapilli and ash beds. The contact between the ash beds and the underlying units is represented by a transitional mixing band with wavelength of decimeters to meters. The upper part of the undulated mixed material shows imbrication of coarser clasts.	The undulated contact between ash and underlying lapilli and ash beds indicates shear exerted by the overriding flows to the loose underlying units, which induces remobilization of its upper part producing imbrication of coarse clasts and formation of waves with variable wavelength. These structures indicate high shear stress exerted by the ash flows to the substratum. Imbrication of coarse clasts testifies for the occurrence of traction carpet processes with remobilisation of the sheared material in a frictional regime.	Figs. 5A-C
rfAL	Recumbent flame structures of lapilli from the underlying beds within the ash units. The upper part of the underlying lapilli bed is ripped up and bended downflow to form an alignement of lapilli within the ash deposit.	Recumbent flame structures indicate high shear exerted by the overriding ash flows over the underlying lapilli beds, which produce incorporation of lapilli that are aligned downflow for a distance up to some meters.	Figs. 5D-E
ruAL	Rip up lapilli from the underlying beds into the ash units. Small hook-like structures visible at the contact between ash and lapilli beds. The main part of the contact is almost planar.	Small hook-like structures indicate moderate shear exerted from the overriding ash flow, which is not able to significantly displace the upper part of the underlying lapilli bed.	Fig. 5F

Table 3 Click here to access/download;Table;Table 3_lucchi.pdf

Table 3. Grain size statistical parameters of Folk and Ward (1957) for the different sub-populations recognised in the samples from the base of some BT depositional units: BT=Brown Tuffs; mg=Monte guardia unit; lpt=Lower Pollara Tuffs; fa=Falcone unit. The parameters by Folk and Ward (1957) were calculated by means of the GRADISTAT program (Blott and Pye, 2001). The Sauter mean diameter (Sauter 1926) of the different BT sub-populations is estimated using the method of Breard et al. (2019).

Sample		LIP02/17		LIP03/17		LIP16/17		LIP20/17		LIP19/17		LIP19a/17		LIP23a/17	
		BT	mg	BT	mg	BT	mg	BT	mg	BT	lpt	BT	lpt	BT	fa
Median	(Mϕ)	1,98	-0,94	3,22	1,34	3,74	-0,76	4,70	-1,45	4,97	0,19	4,73	-0,22	3,13	-0,59
Mean	$(\bar{x})$	2,18	-1,09	3,25	1,05	3,80	-0,66	4,39	-1,29	4,84	0,40	4,62	-0,18	3,04	-0,64
Sorting	(s)	1,71	1,79	1,29	1,35	1,83	2,07	2,10	1,60	1,78	1,32	1,79	1,29	1,53	2,04
Skewness	(Sk)	0,19	-0,07	-0,08	-0,65	-0,29	0,10	-0,72	0,47	-0,63	0,26	-0,25	0,19	-0,28	-0,08
Kurtosis	(K)	0,93	0,89	4,01	2,45	3,40	1,75	3,31	2,65	4,17	2,07	2,69	2,77	3,25	1,89
Sauter number	(D_{32})	0,25		0,11		0,08		0,04		0,03		0,04		0,11	